

ATMOSPHERIC REFRACTION ERRORS
IN LASER RANGING SYSTEMS

by

C. S. Gardner
J. R. Rowlett

RRL Publication No. 477

Final Report
November 1976

Supported by

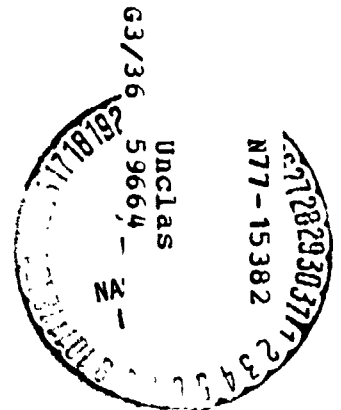
Contract No. NASA NSG 5049

NATIONAL AERONAUTICS & SPACE ADMINISTRATION
Goddard Space Flight Center
Greenbelt, Maryland 20771



RADIO RESEARCH LABORATORY
DEPARTMENT OF ELECTRICAL ENGINEERING
COLLEGE OF ENGINEERING
UNIVERSITY OF ILLINOIS
URBANA, ILLINOIS 61801

(NASA-CR-149281) ATMOSPHERIC REFRACTION
ERRORS IN LASER RANGING SYSTEMS Final
Report (Illinois Univ.) 52 p HC A04/MF A01
CSC 20E



UILU-ENG-77-2538

ATMOSPHERIC REFRACTION ERRORS
IN LASER RANGING SYSTEMS

by

C. S. Gardner
J. R. Rowlett

RRL Publication No. 477

Final Report
November 1976

Supported by

Contract No. NASA NSG 5049

NATIONAL AERONAUTICS & SPACE ADMINISTRATION
Goddard Space Flight Center
Greenbelt, Maryland 20771

RADIO RESEARCH LABORATORY
DEPARTMENT OF ELECTRICAL ENGINEERING
COLLEGE OF ENGINEERING
UNIVERSITY OF ILLINOIS
URBANA, ILLINOIS 61801

ABSTRACT

The effects of horizontal refractivity gradients on the accuracy of laser ranging systems were investigated by ray-tracing through three-dimensional refractivity profiles. The profiles were generated by performing a multiple regression on measurements from seven or eight radiosondes, using a refractivity model which provided for both linear and quadratic variations in the horizontal direction. The range correction due to horizontal gradients was found to be an approximately sinusoidal function of azimuth having a minimum near 0° azimuth and a maximum near 180° azimuth. The peak-to-peak variation was approximately 5 centimeters at 10° elevation and decreased to less than 1 millimeter at 80° elevation.

TABLE OF CONTENTS

	Page
1. INTRODUCTION	1
2. SURFACE CORRECTION FORMULA	2
3. THREE-DIMENSIONAL REFRACTIVITY PROFILE	9
4. RAY-TRACING PROCEDURE.	12
5. RESULTS.	17
5.1 Horizontal Refractivity Gradients	17
5.2 Ray-Tracing Procedure	20
5.3 Three-Dimensional Ray Traces.	25
6. CONCLUSIONS.	38
APPENDIX A. APPROXIMATION OF $\frac{1}{\sin(\theta)}$	39
APPENDIX B. SIMPLIFICATION OF EQUATION (2-9).	41
APPENDIX C. INTEGRAL EVALUATIONS.	43
APPENDIX D. MARINI AND MURRAY'S SURFACE CORRECTION FORMULA.	46
REFERENCES	47

LIST OF FIGURES

Figure	Page
1. Geometry of laser ranging site and satellite target	3
2. Location of balloon release sites for Project Haven Hop I . . .	13
3. Group refractivity N_g , north-south horizontal refractivity gradient $\frac{\partial N_g}{\partial \theta}$, and east-west horizontal refractivity gradient $\frac{1}{\sin(\theta)} \frac{\partial N_g}{\partial \phi}$ directly above site 54 at 1130 GMT 2/16/70	18
4. Group refractivity N_g , north-south horizontal refractivity gradient $\frac{\partial N_g}{\partial \theta}$, and east-west horizontal refractivity gradient $\frac{1}{\sin(\theta)} \frac{\partial N_g}{\partial \phi}$ directly above site 54 at 2330 GMT 1/21/70	19
5. Comparison of RT_3 for tracked ascent and vertical ascent ray traces at 10° elevation.	21
6. Comparison of RT_3 for ray traces using six-coefficient model (Eq. 3-2) and four-coefficient model (Eq. 3-3) at 10° elevation.	24
7. Difference between three-dimensional ray trace (RT_3) and spherically symmetric ray trace (RT_1) at 10° and 20° elevation.	26
8. Difference between three-dimensional ray trace (RT_3) and spherically symmetric ray trace (RT_1) at 40° and 80° elevation.	27
9. Mean of difference $RT_3 - RT_1$ versus azimuth at 10° and 20° elevation (31 sets of data)	29
10. Mean of difference $RT_3 - RT_1$ versus azimuth at 40° and 80° elevation (31 sets of data)	30
11. Standard deviation of difference $RT_3 - RT_1$ versus azimuth at 10° and 20° elevation (31 sets of data)	31
12. Standard deviation of difference $RT_3 - RT_1$ versus azimuth at 40° and 80° elevation (31 sets of data)	32
13. Histogram of difference $RT_3 - RT_1$ at 10° elevation (31 sets of data, 1116 observations)	34

Figure		Page
14.	Histogram of difference $RT_3 - RT_1$ at 20° elevation (31 sets of data, 1116 observations)	35
15.	Histogram of difference $RT_3 - RT_1$ at 40° elevation (31 sets of data, 1116 observations)	36
16.	Histogram of difference $RT_3 - RT_1$ at 80° elevation (31 sets of data, 1116 observations)	37

1. INTRODUCTION

Laser ranging can be used to precisely measure the distance from a point on earth to an orbiting satellite. Ranging accuracy is limited by atmospheric refraction and scattering. In this paper, the effects of atmospheric refraction will be investigated. Atmospheric refraction will increase the optical path length to an orbiting satellite by over 15 meters when the satellite is at 10° elevation, and by about 2 meters when the satellite is directly above the tracking station.

Numerous formulas have been developed to estimate the range error due to refraction. These formulas use surface measurements of pressure, temperature, and relative humidity to predict the range error. The analysis developed by Marini and Murray [1] is used in this paper to derive a new surface correction formula. The formula is derived under the assumption that the atmospheric refractivity is spherically symmetric, that is, the index of refraction is a function of height only. Horizontal refractivity gradients will introduce errors into the surface correction formula. Zanter, Gardner and Rao[2] investigated this effect by ray tracing through a refractivity model having a linear dependence on horizontal position. In this report, a quadratic refractivity model is used to determine the accuracy of the range correction formula by ray tracing at various azimuth and elevation angles.

2. SURFACE CORRECTION FORMULA

The geometry of the laser ranging problem is shown in Fig. 1. The laser pulse travels a curved path from the tracking station (H meters above sea level and r_0 meters from the center of the earth) to the satellite (r_1 meters from the center of the earth). θ_0 is the arrival angle of the pulse, while E is the satellite's actual elevation angle. θ is the angle of the ray with the horizontal (a function of height). The problem is to find R, the straight-line distance to the satellite by measuring the curved distance R_0 .

The derivation of a surface correction formula requires the index of refraction n and the corresponding phase refractivity N [1]:

$$N \equiv 10^6 (n - 1) \\ = \left(287.604 + \frac{1.6288}{\lambda^2} + \frac{0.0136}{\lambda^4} \right) \left(\frac{273.15}{1013.25} \right) \frac{P}{T} - (0.055)(760) \left(\frac{273.15}{1013.25} \right) \frac{e}{T}$$

where λ = wavelength of laser in microns

P = atmospheric pressure in millibars

T = temperature in degrees Kelvin

e = partial pressure of water vapor in millibars.

The group refractivity N_g and group index of refraction n_g must also be known [1]

$$N_g = 10^6 (n_g - 1) = N - \lambda \frac{dN}{d\lambda} \\ = 80.343f(\lambda) \frac{P}{T} - 11.5 \frac{e}{T} \quad (2-1)$$

where $f(\lambda) = 0.9650 + 0.0164/\lambda^2 - 0.000228/\lambda^4$.

According to the theory of geometric optics, the optical path length R_0 is:

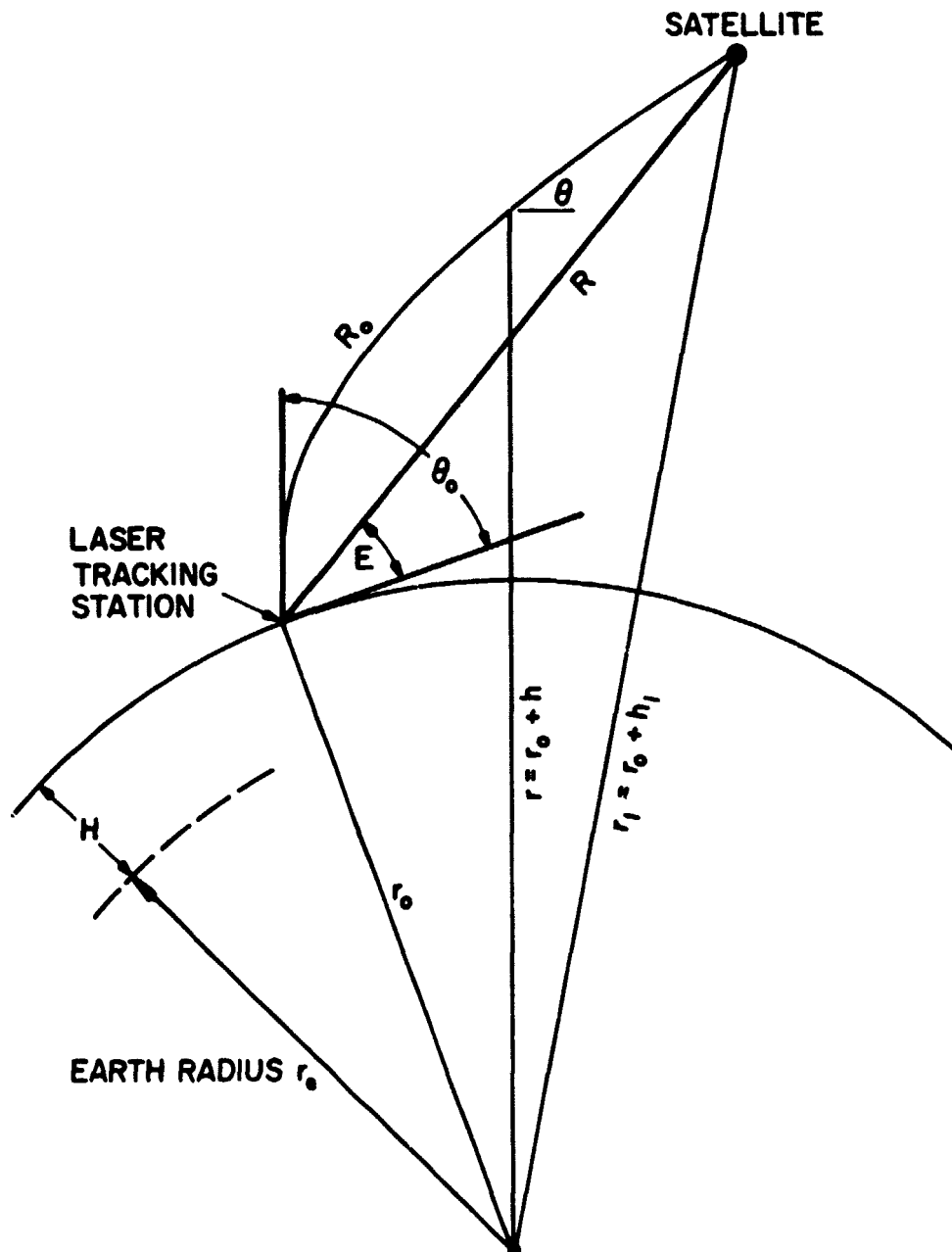


Figure 1. Geometry of laser ranging site and satellite target.

$$R_o = \int_C n_g dl \quad (2-2)$$

where dl is an incremental length along the ray path C . If the group index of refraction is a function of height only (spherical symmetry), the ray path will lie entirely in a plane, and

$$dl = \frac{dr}{\sin(\theta)}$$

so (2-2) becomes

$$\begin{aligned} R_o &= \int_{r_0}^{r_1} \frac{n_g}{\sin(\theta)} dr \\ &= 10^{-6} \int_{r_0}^{r_1} \frac{N_g}{\sin(\theta)} dr + \int_{r_0}^{r_1} \frac{dr}{\sin(\theta)} \end{aligned}$$

The difference between the curved and straight-line distances is the range error ΔR

$$\Delta R = R_o - R = 10^{-6} \int_{r_0}^{r_1} \frac{N_g}{\sin(\theta)} dr + \left[\int_{r_0}^{r_1} \frac{dr}{\sin(\theta)} - R \right] \quad (2-3)$$

The bracketed term corresponds to the geometrical error in path length and has been evaluated in [1]:

$$\int_{r_0}^{r_1} \frac{dr}{\sin(\theta)} - R \approx \frac{1}{\sin^3(\theta_0)} \frac{1}{2} 10^{-12} \int_0^{\infty} N^2 dh \quad (2-4)$$

The first term of (2-3) corresponds to the velocity error. Since the satellite is above the atmosphere ($r_1 > 70$ km) where $N_g \approx 0$, the upper limit can be extended to infinity and a change of variable from r to h gives

$$10^{-6} \int_{r_0}^{r_1} \frac{N_g}{\sin(\theta)} dr = 10^{-6} \int_0^{\infty} \frac{N_g}{\sin(\theta)} dh \quad (2-5)$$

To evaluate the right-hand side of (2-5), Marini and Murray expanded the integrand in inverse powers of $\sin(\theta)$. θ_0 can be related to θ by Snell's law for spherically symmetric media:

$$nr \cos(\theta) = n_0 r_0 \cos(\theta_0).$$

This formula is solved for $\frac{1}{\sin(\theta)}$

$$\frac{1}{\sin(\theta)} = \frac{1}{\sin(\theta_0)} \cdot \frac{1}{\left[1 + \frac{1 - \left(\frac{n_0 r_0}{nr}\right)^2}{\tan^2(\theta_0)} \right]^{1/2}}.$$

$\frac{1}{\sin(\theta)}$ can be expanded using approximations detailed in Appendix A,

$$\frac{1}{\sin(\theta)} = \frac{1}{\sin(\theta_0)} \left\{ 1 - \frac{\frac{h}{r_0} - 10^{-6}(N_0 - N)}{\tan^2(\theta_0)} + \frac{\frac{3}{2} \left[\frac{h}{r_0} - 10^{-6}(N_0 - N) \right]^2}{\tan^4 \theta_0} \right\}. \quad (2-6)$$

Using (2-5) and (2-6) in (2-3), we obtain

$$\begin{aligned} \Delta R = & \frac{1}{\sin(\theta_0)} \left\{ 10^{-6} \int N_g dh + 10^{-6} \int \left[\frac{h}{r_0} - 10^{-6}(N_0 - N) \right] N_g dh \right. \\ & + \frac{3}{2} \cdot 10^{-6} \int \left[\frac{h}{r_0} - 10^{-6}(N_0 - N) \right]^2 N_g dh \left. \right\} \\ & - \frac{1}{\sin^3(\theta_0)} \left\{ 10^{-6} \int \left[\frac{h}{r_0} - 10^{-6}(N_0 - N) \right] N_g dh - \frac{1}{2} \cdot 10^{-12} \int N^2 dh \right. \\ & + 3 \cdot 10^{-6} \int \left[\frac{h}{r_0} - 10^{-6}(N_0 - N) \right]^2 N_g dh \left. \right\} \\ & + \frac{1}{\sin^5(\theta_0)} \left\{ \frac{3}{2} \cdot 10^{-6} \int \left[\frac{h}{r_0} - 10^{-6}(N_0 - N) \right]^2 N_g dh \right\}. \quad (2-7) \end{aligned}$$

Marini and Murray express their result in terms of the actual satellite elevation angle E rather than the arrival angle θ_0 . The conversion can be

* Unless otherwise noted, the limits on all integrals in this report will be from 0 to ∞ .

made using the first term of the angular correction. [1]:

$$\theta_0 - E \approx 10^{-6} N_0 \cot (E) .$$

Adding E to both sides and taking the sine

$$\sin (\theta_0) \approx \sin \left[E + 10^{-6} N_0 \cot (E) \right]$$

$N_0 \approx 300$, so for $E \geq 10^\circ$, $10^{-6} N_0 \cot (E)$ is small, and

$$\begin{aligned} \sin (\theta_0) &\approx \sin (E) + 10^{-6} N_0 \cot (E) \cos (E) \\ \frac{1}{\sin (\theta_0)} &\approx \frac{1}{\sin (E)} - \frac{10^{-6} N_0 \cot (E) \cos (E)}{\sin^2 (E) + 10^{-6} N_0 \cos^2 (E)} . \end{aligned}$$

Now $10^{-6} N_0 \cos^2 (E) \ll \sin (E)$ for $E \geq 10^\circ$, giving

$$\begin{aligned} \frac{1}{\sin (\theta_0)} &\approx \frac{1}{\sin (E)} - \frac{10^{-6} N_0 [1 - \sin^2 (E)]}{\sin^3 (E)} \\ &\approx \frac{1}{\sin (E)} - \frac{10^{-6} N_0}{\sin^3 (E)} . \end{aligned} \quad (2-8)$$

Applying (2-8) to (2-7), we obtain

$$\begin{aligned} \Delta R &\approx \frac{1}{\sin (E)} \left\{ 10^{-6} \int N_g dh + 10^{-6} \int \left[\frac{h}{r_0} - 10^{-6} (N_0 - N) \right] N_g dh \right. \\ &\quad \left. + \frac{3}{2} \cdot 10^{-6} \int \left[\frac{h}{r_0} - 10^{-6} (N_0 - N) \right]^2 N_g dh \right\} \\ &\quad - \frac{1}{\sin^3 (E)} \left\{ 10^{-12} N_0 \int \left[\frac{h}{r_0} - 10^{-6} (N_0 - N) \right] N_g dh \right. \\ &\quad \left. + \frac{10^{-6}}{r_0} \int h N_g dh + 10^{-12} \int \left[N N_g - \frac{1}{2} N^2 \right] dh \right. \\ &\quad \left. + 3 \times 10^{-6} \int \left[\frac{h}{r_0} - 10^{-6} (N_0 - N) \right]^2 N_g dh \right\} \\ &\quad + \frac{1}{\sin^5 (E)} \left\{ 3 \times 10^{-12} N_0 \int \left[\frac{h}{r_0} + 10^{-6} N + 3 \left[\frac{h}{r_0} - 10^{-6} (N_0 - N) \right]^2 \right] N_g dh \right. \\ &\quad \left. + \frac{3}{2} \cdot 10^{-6} \int \left[\frac{h}{r_0} + 10^{-6} (N_0 - N) \right]^2 N_g dh \right\} . \end{aligned} \quad (2-9)$$

Many of the terms in (2-9) can be ignored, as they either make a contribution of less than 1 mm to ΔR at $E = 10^\circ$, or they cancel each other. Making these simplifications, which are detailed in Appendix B,

$$\begin{aligned} \Delta R \approx & \frac{1}{\sin(E)} \left[\frac{10^{-6} \int N_g dh + \frac{10^{-6}}{r_0} \int h N_g dh - 10^{-12} \int (N_0 - N) N_g dh \right] \\ & - \frac{1}{\sin^3(E)} \left[\frac{10^{-6}}{r_0} \int h N_g dh + 10^{-12} \int \left(N N_g - \frac{1}{2} N^2 \right) dh \right] \\ & + \frac{1}{\sin^5(E)} \left[\frac{3}{2} \cdot \frac{10^{-6}}{r_0^2} \int h^2 N_g dh \right] . \end{aligned} \quad (2-10)$$

The underlined terms in (2-10) appear in the correction formula developed by Marini and Murray [1] and have been evaluated by them. The last integral in (2-10) was not used by Marini and Murray and is evaluated in Appendix C. The integral evaluations, taken from Marini and Murray [1] and Appendix C. are:

$$\begin{aligned} 10^{-6} \int N_g dh & \approx \frac{f(\lambda)}{F(\theta, H)} [0.002357 P_s + 0.000141 e_s] \\ \frac{10^{-6}}{r_0} \int h N_g dh & \approx 1.0842 \times 10^{-8} f(\lambda) P_s T_s K \\ 10^{-12} \int (N_0 - N) N_g dh & \approx 9.4682 \times 10^{-8} f(\lambda) \frac{P_s^2}{T_s} \\ 10^{-12} \int \left(N N_g - \frac{1}{2} N^2 \right) dh & \approx 4.7343 \times 10^{-8} f(\lambda) \frac{P_s^2}{T_s} \frac{2}{3 - 1/K} \\ \frac{3}{2} \frac{10^{-6}}{r_0^2} \int h^2 N_g dh & \approx 1.4961 \times 10^{-13} f(\lambda) P_s T_s^2 \frac{K^2}{2 - K} \end{aligned} \quad (2-11)$$

$$\text{where } f(\lambda) = 0.9650 + \frac{0.0164}{\lambda^2} + \frac{0.000228}{\lambda}$$

$$F(\theta, H) = 1 + 0.0026 \cos(2\theta) - 0.00031H$$

$$K = 63 + 0.00968 \cos(2\theta) - 0.00104 T_s + 0.0001435 P_s$$

$$\theta = \text{latitude of laser site}$$

H = surface height at laser site (in km)

P_s = surface pressure at laser site (in mb)

T_s = surface temperature at laser site (in °K)

e_s = surface partial pressure of water vapor at laser site (in mb)

λ = wavelength of laser (in microns).

Equation (2-10) can be expressed in a continued fraction form, similar to that used by Marini and Murray [1]

$$\begin{aligned} \Delta R &= f(\lambda) \left[\frac{A}{\sin(E)} - \frac{B}{\sin^3(E)} + \frac{C}{\sin^5(E)} \right] \\ &= f(\lambda) \frac{A}{\sin(E) + \frac{B/A}{\sin(E) + \frac{C/B}{\sin(E) + 0.17}}} \end{aligned} \quad (2-12)$$

$$\begin{aligned} \text{where } A &= \frac{1}{F(\theta, H)} [0.002357P_s + 0.000141e_s] + 1.0842 \times 10^{-8} P_s T_s K \\ &\quad - 9.4682 \times 10^{-8} \frac{P_s^2}{T_s} \end{aligned}$$

$$B = 1.0842 \times 10^{-8} P_s T_s K + 4.7343 \times 10^{-8} \frac{P_s^2}{T_s} \frac{2}{3 - 1/K}$$

$$C = 1.4961 \times 10^{-13} P_s T_s^2 \frac{K^2}{2 - K}$$

The 0.17 is an empirical constant which compensates for approximations made in the derivation of (2-12). The surface correction formula developed by Marini and Murray [1] contains an empirical constant (0.01) which replaces the term $\frac{C/B}{\sin(E) + 0.17}$ in (2-12) (see Appendix D).

3. THREE-DIMENSIONAL REFRACTIVITY PROFILE

Marini and Murray compared their formula with a range correction obtained by ray tracing through a spherically symmetric atmosphere. The assumption of spherical symmetry means that the refractivity is a function of height only (independent of horizontal position). Any nonsymmetric behavior of the atmosphere would introduce errors in a ray trace made under the spherical symmetry assumption.

To investigate the errors introduced by this assumption, Zanter, Gardner and Rao [2] assumed that the refractivity at a given height had a linear dependence on position:

$$N = N_r + \theta N_\theta + \phi \sin(\theta) N_\phi \quad (3-1)$$

where N = refractivity

θ = colatitude = 90° - latitude

ϕ = longitude

N_r, N_θ, N_ϕ = coefficients to be determined for each height.

θ is proportional to horizontal displacement in the north-south direction, while $\phi \sin \theta$ is proportional to horizontal displacement in the east-west direction. The three coefficients can be determined at any particular altitude from a knowledge of the refractivity at a minimum of three points at that altitude.

Refractivity does not exactly follow the linear model of (3-1), and a more accurate quadratic model was used for this investigation:

$$N = N_r + \theta N_\theta + \phi \sin(\theta) N_\phi + \theta \phi \sin(\theta) N_{\theta\phi} + \theta^2 N_{\theta\theta} + \phi^2 \sin^2(\theta) N_{\phi\phi} \quad (3-2)$$

The six coefficients can be determined at a particular altitude from a minimum of six refractivity measurements.

Refractivity is calculated from radiosonde measurements of pressure, temperature, and relative humidity. Errors in radiosonde pressure and temperature measurements tend to be magnified by the quadratic terms of (3-2). Because the rms radiosonde errors are constant rather than a percentage of the measurement, the errors have a greater effect at higher altitudes where the measurement values are smaller. For instance, the rms pressure error at sea level is about 0.1 percent of the ambient pressure, but at 15 km altitude the rms error has grown to 1 percent of the ambient pressure [2].

The effects of measurement errors are minimized by using more than the minimum of six radiosonde balloons and performing a multiple regression to find the refractivity coefficients N_r , N_θ , N_ϕ , $N_{\theta\phi}$, $N_{\theta\theta}$, $N_{\phi\phi}$ [3]. In this investigation eight radiosonde profiles were used, providing a regression with two degrees of freedom.

Most of the radiosonde data end at a height of about 15 km, and refractivity above the cut-off point must be extrapolated (see Section 4). Because of the extrapolation and the greater effects of measurement errors at higher altitudes, a four-coefficient model is used at heights above 15 km.

$$N = N_r + \theta N_\theta + \phi \sin(\theta) N_\phi + \theta\phi \sin(\theta) N_{\phi\phi} \quad (3-3)$$

This model gives four degrees of freedom in the regression at the more critical higher altitudes with little sacrifice in accuracy, since refractivity is more uniform at these heights than it is near the surface.

Because of balloon malfunctions, only about twenty sets of data with eight radiosonde profiles were available. Ten additional sets with seven profiles were available. However, the quadratic model of (3-2) would have provided only a single degree of freedom in the regression. To reduce the effects of radiosonde measurement errors in these seven-station sets, the four-coefficient model (3-3) was used at all altitudes.

Using the appropriate model, (3-2) or (3-3), multiple regression is used to find the coefficients at each height from refractivity measurements at that height. Once the coefficients have been determined, they can be used to calculate the refractivity along a ray in any direction.

A ray trace which uses a spherically symmetric refractivity profile is employed to test the accuracy of the surface correction formula. Marini and Murray obtained a spherically symmetric profile from measurements made by a single radiosonde. However, the regression coefficients can also be used to obtain a spherically symmetric profile. The profile is generated by calculating the refractivity directly above the laser site, using the regression coefficients. This approach tends to minimize the effects of errors in the radiosonde data, and is therefore more accurate than simply using the measurements made by a single radiosonde.

4. RAY-TRACING PROCEDURE

The data used to construct refractivity profiles were gathered in Project Haven Hop I during January and February of 1970 [4]. The Haven Hop data consist of measurements of pressure, temperature, and relative humidity made by radiosonde balloons released from sites in the Washington, D.C. area (see Figure 2). The balloons were released from the sites within a few minutes of each other at various times during the night and day and tracked to an average altitude of about 15 km. The radiosondes report observations of pressure, temperature, and relative humidity every 30 seconds as they ascend. From these observations, the phase refractivity and group refractivity can be calculated.

The refractivity must be known at certain standard altitudes between the surface and 1000 km, the assumed satellite height. For altitudes below the radiosonde cut-off point, the radiosonde measurements are interpolated to the nearest standard altitude, following the procedure in Zanter, Gardner and Rao [2]. The radiosonde heights are inferred from the measurements using the hydrostatic equation. Above the radiosonde cut-off, the last measurements must be extrapolated. As is done in Zanter et al. [2], pressure is assumed to decay exponentially, while temperature and relative humidity remain constant. Once the pressure, temperature, and relative humidity are known at the standard altitudes, the refractivity can be calculated.

Some error is introduced because the radiosonde balloons take from 45 minutes to an hour to ascend, whereas a laser pulse would pass through the atmosphere almost instantaneously. This problem can be dealt with in either of two ways:

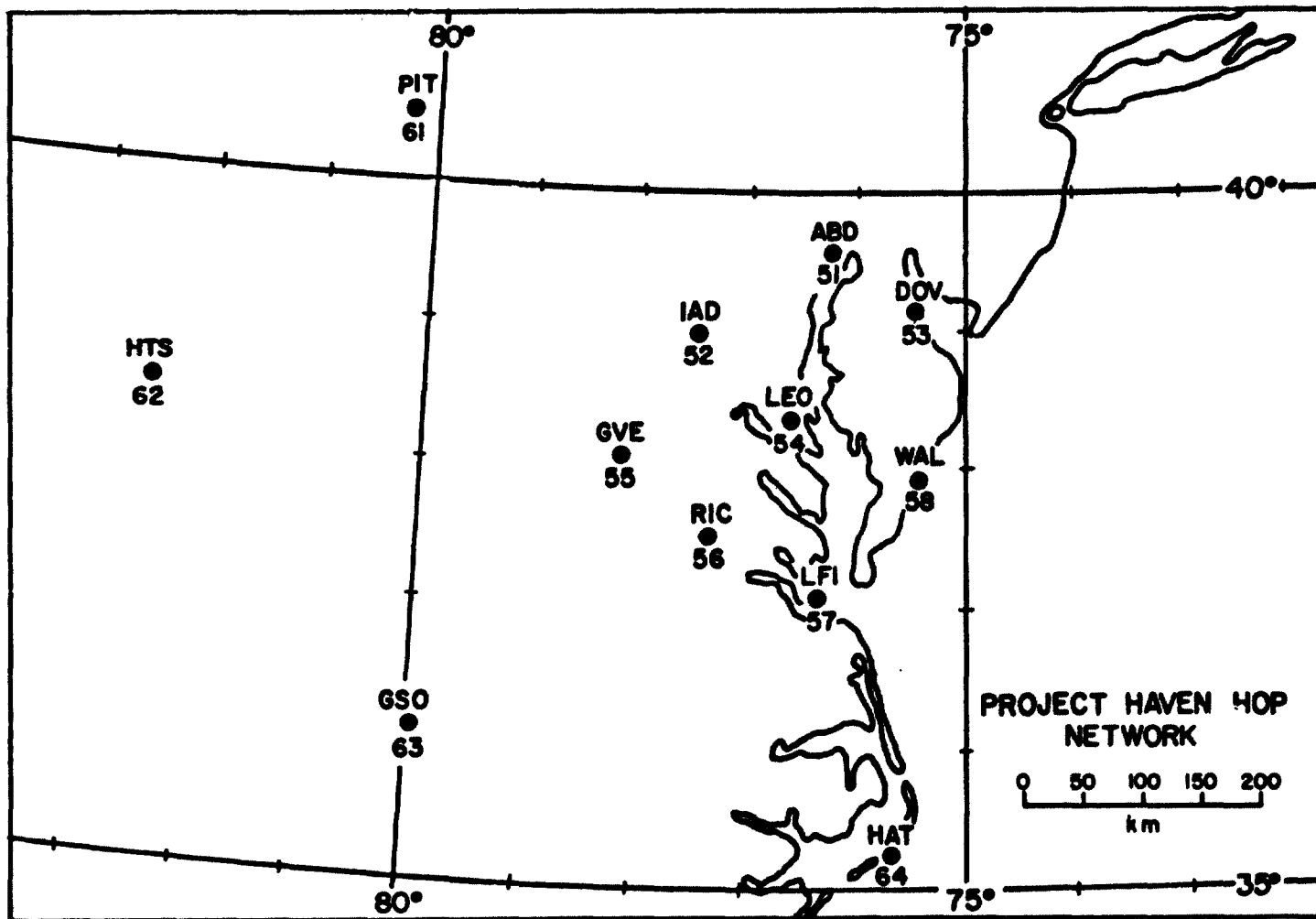


Figure 2. Location of balloon release sites for Project Haven Hop I. Laser ranging site = 54.

- (1) It can be argued that the atmosphere does not change significantly under normal conditions during ascent, so the ascent time can be neglected. In this case, the tracking data are used to determine the radiosonde position as it is blown downrange during ascent (tracked ascent).
- (2) Since the balloons ascend on an approximately linear path (that is, wind speed and direction are nearly constant at all altitudes), the measurements taken along the balloon path are a good estimate of the conditions directly above the release site at the instant the balloon started its ascent. In this case, tracking data are ignored, and the balloons are assumed to ascend directly above the tracking site (vertical ascent).

Since neither argument is entirely satisfactory, ray traces were made under both assumptions. The difference between ray traces on the same set of data under the two assumptions was small (see Section 5).

At each standard height, a multiple regression is performed, using the eight refractivity measurements^{*} and corresponding positions in the appropriate refractivity model, (3-2) or (3-3). A three-dimensional refractivity profile is thus constructed from the eight radiosonde profiles, which allows one to compute the refractivity along any arbitrary ray path. A ray path is specified by azimuth and elevation angles from the release site.

Given an azimuth angle and an elevation angle from the release site, the regression coefficients and the appropriate model of Section 3 are used to generate a refractivity profile along the specified path. This profile is then passed to a ray-tracing program, which computes the range error. Three types of ray traces are made for each set of data:

* Some sets of data contained only seven radiosonde releases, as explained in Section 3.

- (1) Single Radiosonde Spherically Symmetric Ray Trace (RT_{MM}) -
 RT_{MM} uses only the data obtained by the radiosonde released from the laser site. Such a ray trace was used by Marini and Murray to test the accuracy of their surface correction formula. RT_{MM} is made under the assumption of a spherically symmetric atmosphere. In this report, RT_{MM} is used to establish agreement with Marini and Murray.
- (2) Spherically symmetric ray trace (RT_1) - Although RT_{MM} is made under the assumption of a spherically symmetric atmosphere, the use of data from a single radiosonde may cause significant errors in the range correction obtained [2]. RT_1 uses a spherically symmetric refractivity profile obtained by calculating the refractivity directly above the laser site using the three-dimensional regression profile. This approach tends to minimize the effects of radiosonde measurement errors (see Section 3). Since spherical symmetry is assumed, RT_1 is independent of azimuth, and is not sensitive to the effects of horizontal refractivity gradients. RT_1 is used to test the accuracy of the surface correction formula derived in Section 3.
- (3) Three-dimensional ray trace (RT_3) - RT_3 uses the three-dimensional regression coefficients to generate a refractivity profile along the ray path. RT_3 is dependent on azimuth and contains the effects of horizontal refractivity gradients. Since RT_1 contains no gradient effects, the difference $RT_3 - RT_1$ isolates the contribution of gradients to the range correction. Rays are traced every 10° azimuth to find the effects of horizontal refractivity gradients.

Each of the three types of ray traces is made at four different elevation angles: 10°, 20°, 40°, and 80°. The centrally located Leonardtown, Md. station (Site 54) was used as the laser site, so that rays could be traced at all azimuths. The ray-trace routine employed in this report is the Thayer method [5]. This same method was also used by Marini and Murray [1] and Zanter, Gardner and Rao [2]. Agreement with the results obtained by Marini and Murray was checked by feeding the radiosonde data appearing in Appendix 4 of their report into the ray-tracing program. The range correction obtained (RT_{MM}) agreed with that reported by Marini and Murray.

5. RESULTS

5.1 Horizontal Refractivity Gradients

A spherically symmetric atmosphere would have horizontal gradients equal to zero. As stated earlier, nonsymmetric behavior of the atmosphere will introduce errors into the surface correction formula and in any ray trace made under the assumption of spherical symmetry.

The horizontal refractivity gradients can be easily computed from the refractivity model (3-2):

$$\frac{\partial N}{\partial \theta} = N_{\theta} + \phi \cos (\theta) N_{\phi} + [\theta \cos (\theta) + \sin (\theta)] \phi N_{\theta \phi} + 2 \theta N_{\theta \theta} + \phi^2 \sin (2 \theta) N_{\phi \phi} \quad (5-1)$$

$$\frac{\partial N}{\partial \phi} = \sin (\theta) N_{\phi} + \theta \sin (\theta) N_{\theta \phi} + 2 \phi \sin^2 (\theta) N_{\phi \phi} \quad (5-2)$$

where θ is proportional to horizontal displacement in a north-south direction, and $\phi \sin \theta$ is proportional to horizontal displacement in an east-west direction.

Figures 3 and 4 are sample plots of the refractivity and the north-south and east-west gradients versus height. The gradients were calculated for points directly above the laser site. The magnitude of the north-south gradient is generally larger than that of the east-west gradient. This is to be expected, since temperature has a large north-south gradient and refractivity is inversely proportional to temperature. For the Haven Hop data, surface pressure is approximately constant, while surface temperature increases to the south and east. We would expect refractivity to decrease to the south and east, and consequently, both the north-south and east-west gradients to be negative. Both figures confirm our expectation.

In both figures, the north-south gradient reverses sign as height increases. The sign reversal is predicted by the hydrostatic equation: from Appendix C we may write

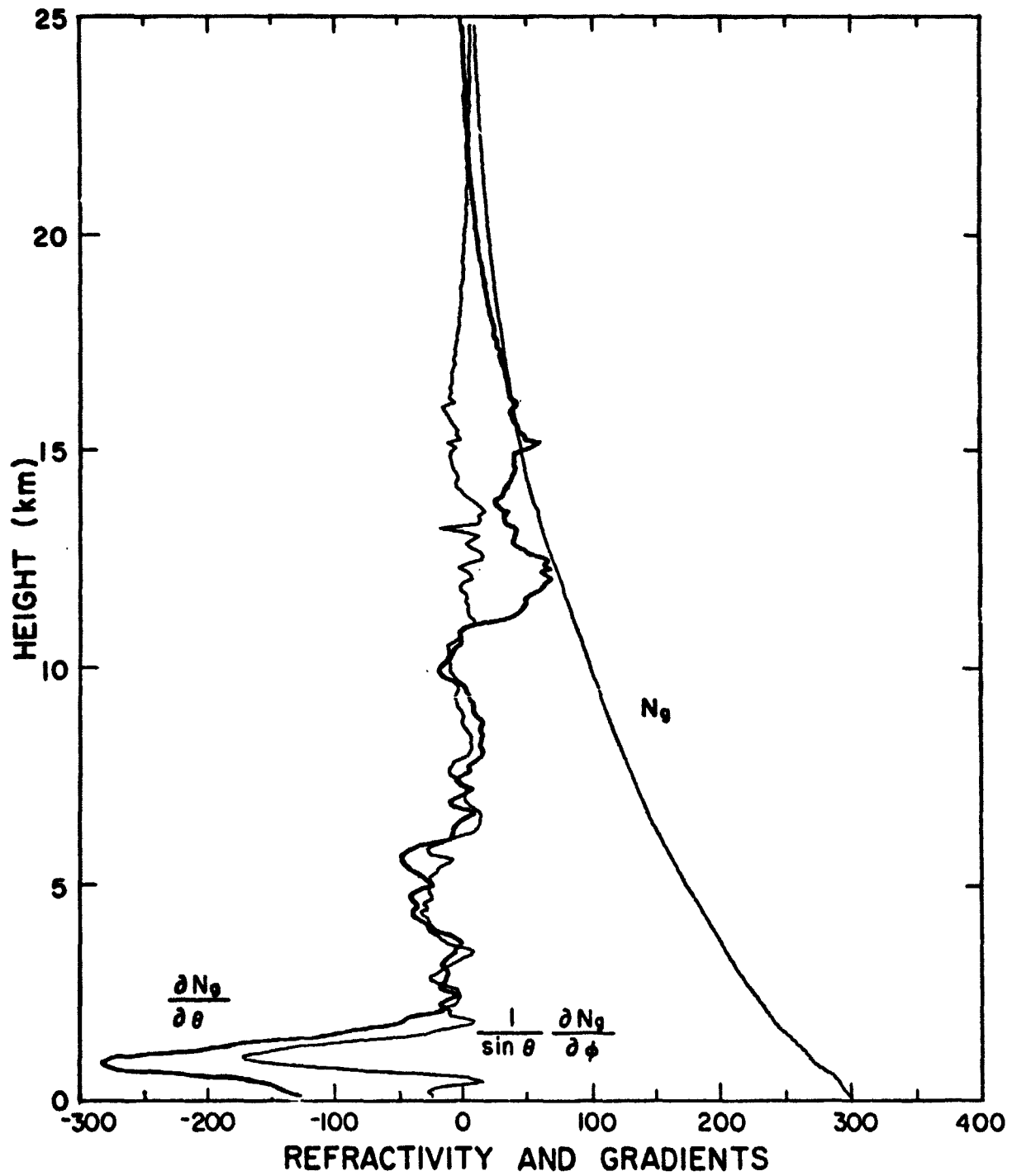


Figure 3. Group refractivity N_g , north-south horizontal refractivity gradient $\frac{\partial N_g}{\partial \theta}$, and east-west horizontal refractivity gradient $\frac{1}{\sin(\theta)} \frac{\partial N_g}{\partial \phi}$ directly above site 54 at 1130 GMT on 2/16/70.

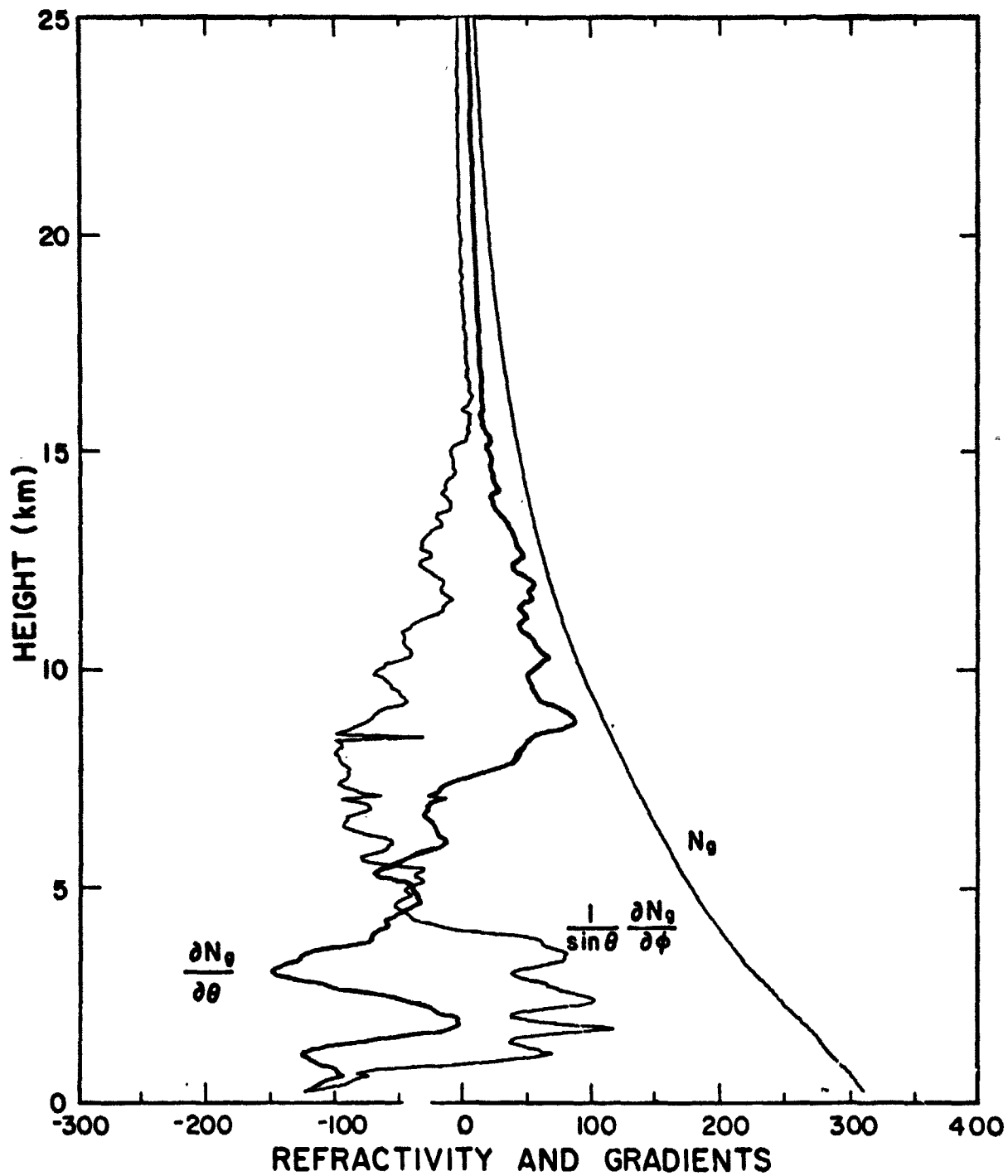


Figure 4. Group refractivity N_g , north-south horizontal refractivity gradient $\frac{\partial N_g}{\partial \theta}$, and east-west horizontal refractivity gradient $\frac{1}{\sin(\theta)} \frac{\partial N_g}{\partial \phi}$ directly above site 54 at 2330 GMT on 1/21/70.

$$P = P_s \left(\frac{T}{T_s} \right)^{-Mg/R\beta}$$

$$T = T_s + \beta h .$$

Approximating refractivity by the dominant first term of (2-1), we obtain

$$N_g = 80.343f(\lambda) \frac{P_s}{T_s} \left(1 + \frac{\beta h}{T_s} \right)^{-(Mg/R\beta+1)} .$$

Then taking the derivative in a horizontal direction,

$$N'_g = N_g \left\{ \frac{P'_s}{P_s} + \frac{T'_s}{T_s} \left[\frac{\frac{\beta}{T_s} h}{1 + \frac{\beta}{T_s} h} \left(\frac{Mg}{R\beta} + 1 \right) - 1 \right] \right\} \quad (5-3)$$

where N'_g , P'_s , T'_s are horizontal gradients of group refractivity, surface pressure, and surface temperature.

If the pressure gradient is ignored, (5-3) predicts a sign reversal at $h = \frac{R}{Mg} T_s$ meters, or about 8 km, which is consistent with Saastamoinen's [6] results.

5.2 Ray-Tracing Procedure

In Section 4 it was pointed out that the ascent time of the radiosondes introduces an error into the ray-trace calculations, since the measurements are not taken at all altitudes simultaneously. One way of dealing with this problem is to assume that the measurements at a point are a good estimate of the conditions there at the instant of balloon release (tracked ascent). The other is to assume that the measurements are a good estimate of conditions directly above the release site, in which case the balloon is assumed to ascend vertically. Ray traces for seventeen sets of data were made under both assumptions for comparison. The results are presented in Table 1, and a sample comparison of three-dimensional ray traces for the same set of data is shown in Figure 5. There is very little

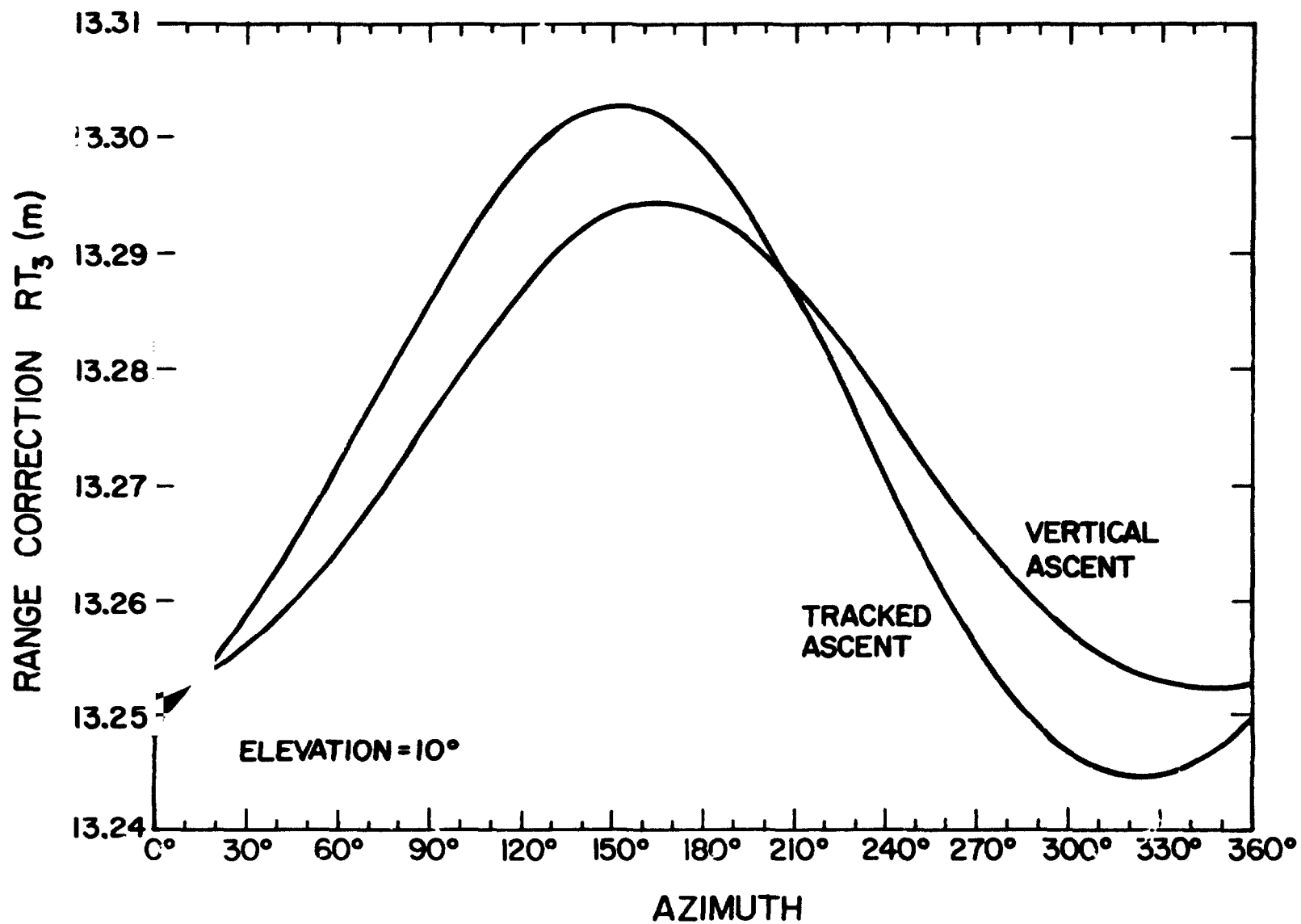


Figure 5. Comparison of RT_3 for tracked ascent and vertical ascent ray traces at 10° elevation.. Balloons released at 1730 GMT on 1/30/70.

difference between the two assumptions. However, since not all balloon releases were tracked, some sets of data could only be processed using vertical ascent ray traces. Furthermore, Gardner and Hendrickson's results appear to agree slightly better with the vertical ascent ray traces [7]. Therefore, the remaining results presented used vertical ascent ray traces.

TABLE 1.

COMPARISON OF SPHERICALLY SYMMETRIC RAY TRACES
USING TRACKED ASCENT AND VERTICAL ASCENT (17 SETS)

<u>Elevation</u>	RT_1 (vertical) - RT_1 (tracked)	
	<u>Mean (cm)</u>	<u>SD (cm)</u>
10°	.29	.75
20°	.11	.46
40°	.06	.25
80°	.04	.16

The surface correction formula derived by Marini and Murray [1] (see Appendix D) was designed to agree with the single radiosonde spherically symmetric ray trace RT_{MM} . However, as seen in Table 2, a bias exists between RT_1 and RT_{MM} . Since RT_1 uses the regression coefficients and is thus less sensitive to radiosonde measurement errors than RT_{MM} , the surface correction formula developed in Section 2 was designed to agree with RT_1 . The error in Marini and Murray's formula (MM) is given by $MM - RT_{MM}$, while the error in the formula of Section 2 (AR) is given by $AR - RT_1$. These errors are compared in Table 2. While the errors in both formulas have about the same standard deviation, the formula of Section 2 has a near zero mean, while Marini and Murray's formula has a bias. This bias was also observed by Zanter, Gardner and

TABLE 2.

COMPARISON OF SPHERICALLY SYMMETRIC RAY TRACES

Elevation	$RT_1 - RT_{MM}$ (24 sets)		$MM - RT_{MM}$ (24 sets)		$\Delta R - RT_1$ (31 sets)	
	Mean (cm)	SD (cm)	Mean (cm)	SD (cm)	Mean (cm)	SD (cm)
10°	0.54	0.75	-0.40	0.49	-0.03	0.46
20°	0.29	0.40	-0.25	0.25	0.06	0.25
40°	0.15	0.21	-0.20	0.14	0.00	0.14
80°	0.10	0.13	-0.13	0.09	0.01	0.09

RT_1 = spherically symmetric ray trace range correction

RT_{MM} = single radiosonde spherically symmetric ray trace range correction

MM = range correction predicted by Marini and Murray's formula

ΔR = range correction predicted by surface correction formula in Section 2.

Ten of the thirty-one available sets of data contained only seven radiosonde releases rather than eight, and these sets were processed using the four-coefficient refractivity model [Eq. (3-3)] to reduce the error in the regression coefficients. To examine the differences between ray traces processed using the six-coefficient model [Eq. (3-2)] and those using the four-coefficient model, another ten sets of data containing eight radiosonde releases were processed twice — once using the six-coefficient model and once using the four-coefficient model. The results are summarized in Table 3, and a sample plot of RT_3 vs. azimuth for the same set of data using each model appears in Figure 6.

The four-coefficient model shows very close agreement with the six-coefficient model, particularly in the means, which are near zero. The

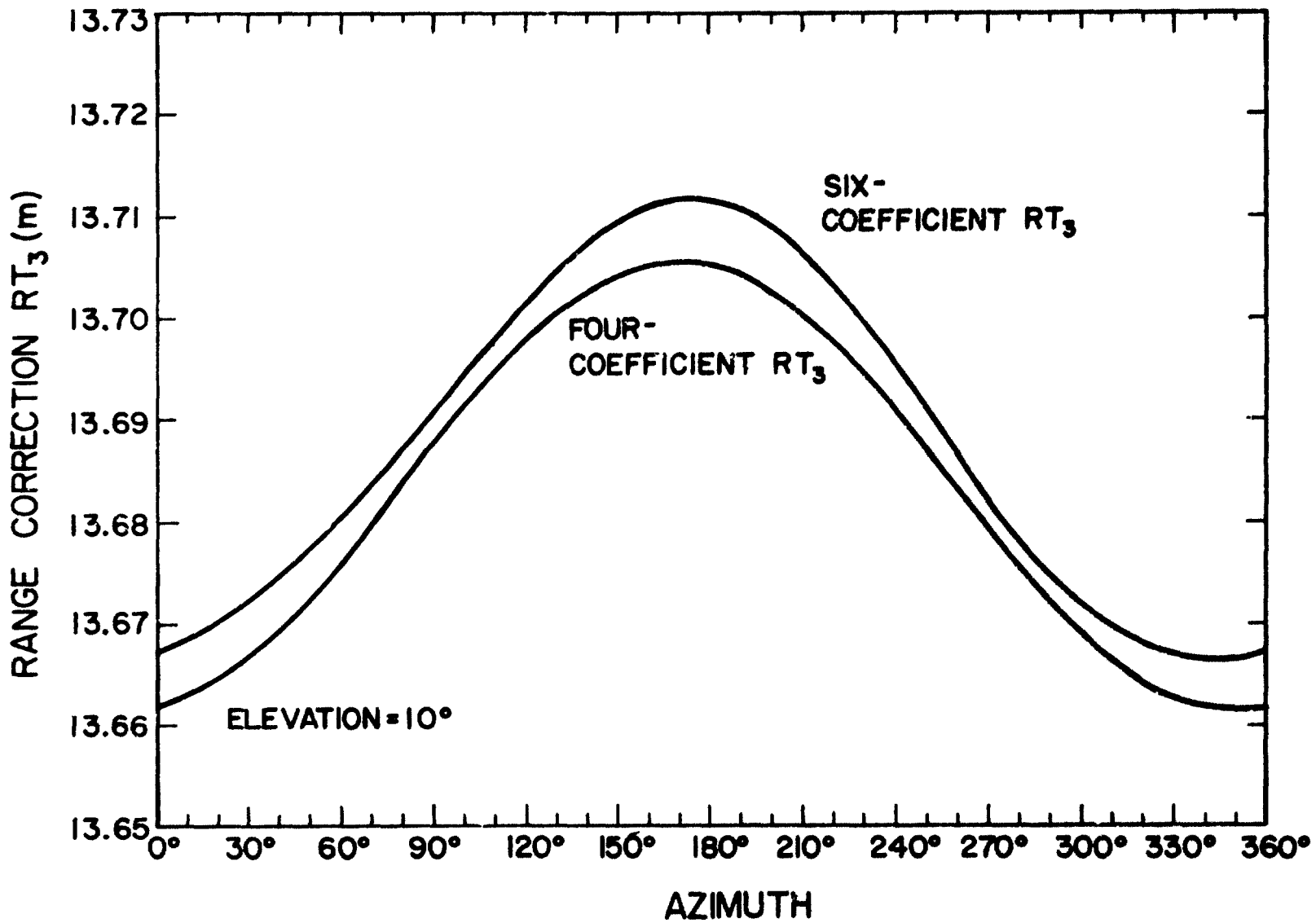


Figure 6. Comparison of RT_3 for ray traces using six-coefficient model (Eq. 3-2) and four coefficient model (Eq. 3-3) at 10° elevation. Balloons released at 1530 GMT on 2/16/70.

four-coefficient ray traces agree extremely closely in gradient effects ($RT_3 - RT_1$) with the six-coefficient model. The extra quadratic terms of Eq. (3-2) apparently contain little information about the horizontal gradients, and so the predominant gradient effects appear to be linear.

TABLE 3.

COMPARISON OF SIX-COEFFICIENT AND FOUR-COEFFICIENT MODELS (10 SETS)

Elevation	$RT_1(6) - RT_1(4)$		$RT_3(6) - RT_3(4)$		$[RT_3 - RT_1](6) - [RT_3 - RT_1](4)$	
	Mean (cm)	SD (cm)	Mean (cm)	SD (cm)	Mean (cm)	SD (cm)
10°	0.09	0.85	0.00	0.79	-0.09	0.29
20°	0.05	0.43	0.04	0.40	-0.01	0.06
40°	0.03	0.23	0.02	0.21	0.00	0.01
80°	0.02	0.15	0.02	0.14	0.00	0.01
No. of Obs.	10		360		360	

5.3 Three-Dimensional Ray Traces

For each set of data, a three-dimensional ray trace RT_3 is made at every 10° azimuth from the laser site for each of four elevation angles: $E = 10^\circ, 20^\circ, 40^\circ, 80^\circ$. The effects of horizontal refractivity gradients are isolated by subtracting the spherically symmetric range error RT_1 , which is independent of azimuth, from the three-dimensional range error RT_3 at each azimuth angle. Sample plots of $RT_3 - RT_1$ vs. azimuth appear in Figures 7 and 8.

The $E = 80^\circ$ curve shows the effects of computer round-off noise, since the refractivity differences computed in the ray trace routine are quite small. Except at $E = 80^\circ$, the range error is an approximately sinusoidal function of azimuth, having a maximum towards the south and a minimum

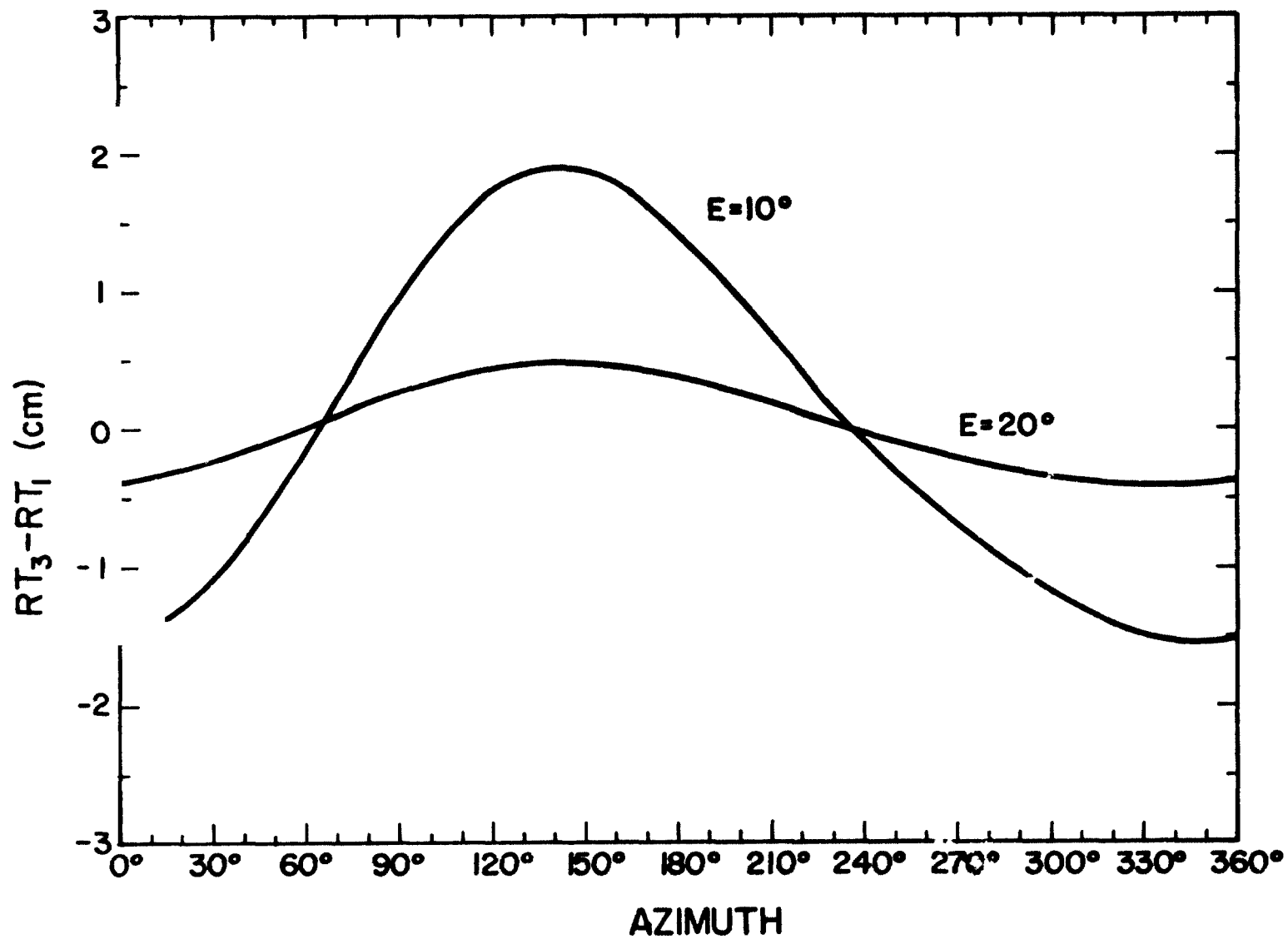


Figure 7. Difference between three-dimensional ray trace (RT_3) and spherically symmetric ray trace (RT_1) at 10° and 20° elevation. Balloons released at 1130 GMT on 2/16/70. 26

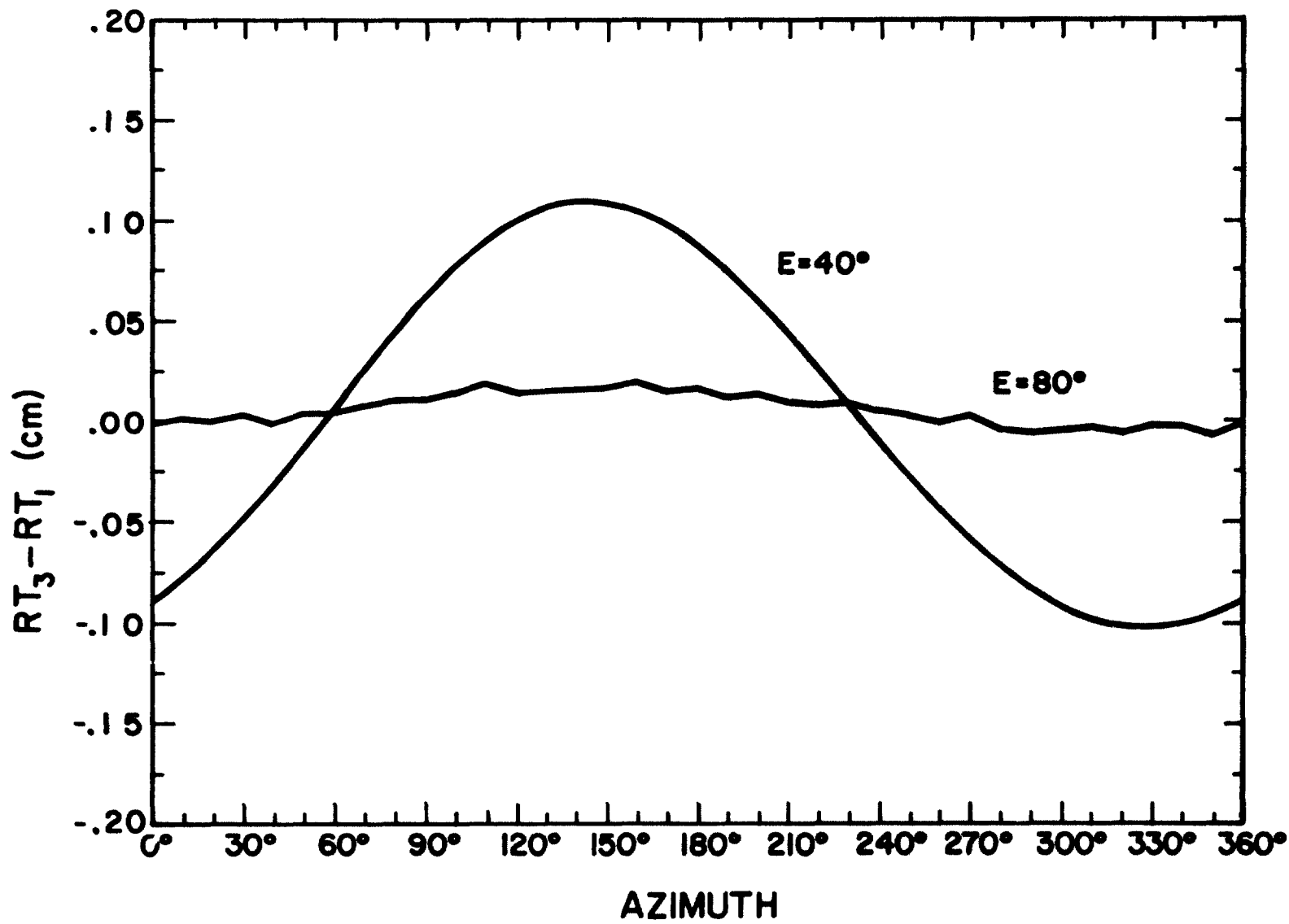


Figure 8. Difference between three-dimensional ray trace (RT_3) and spherically symmetric ray trace (RT_1) at 40° and 80° elevation. Balloons released at 1130 GMT on 2/16/70.

towards the north. One might expect just the opposite, since at the surface there are colder temperatures, and therefore larger values of refractivity to the north. If the north-south refractivity gradient remained negative at all altitudes, one would expect to trace through denser air to the north than to the south, and consequently to have a larger range error to the north. However, as noted earlier, the north-south gradient changes sign around 8 km. The positive gradients above 8 km overcome the effects of the negative gradients near the surface, because the refractivity differences are smaller near the release site than they are at higher altitudes further from the site. Thus, even though the refractivity itself is large at lower altitudes, the contribution to the range error is from refractivity differences, which are small.

The means and standard deviations of $RT_3 - RT_1$ combined over all azimuths for the thirty-one sets of data appear in Table 4. The means are all very close to zero, and so the difference $RT_3 - RT_1$ is a good measure of the effects of horizontal refractivity gradients. The effects of these gradients are quite significant at the lower elevation angles. The means and standard deviations of $RT_3 - RT_1$ for each azimuth angle are plotted in Figures 9-12. At $E = 10^\circ$, the mean swings ± 2.5 cm, but the swing drops to less than ± 0.2 mm at $E = 30^\circ$. The mean curves are very close to being sinusoidal, except at $E = 80^\circ$. The standard deviation appears to be a function of azimuth. However, this effect is due to the limited number of surface stations available (seven or eight) and the regression used in performing the ray trace. The regression error is discussed in detail in Gardner and Hendrickson's report [7].

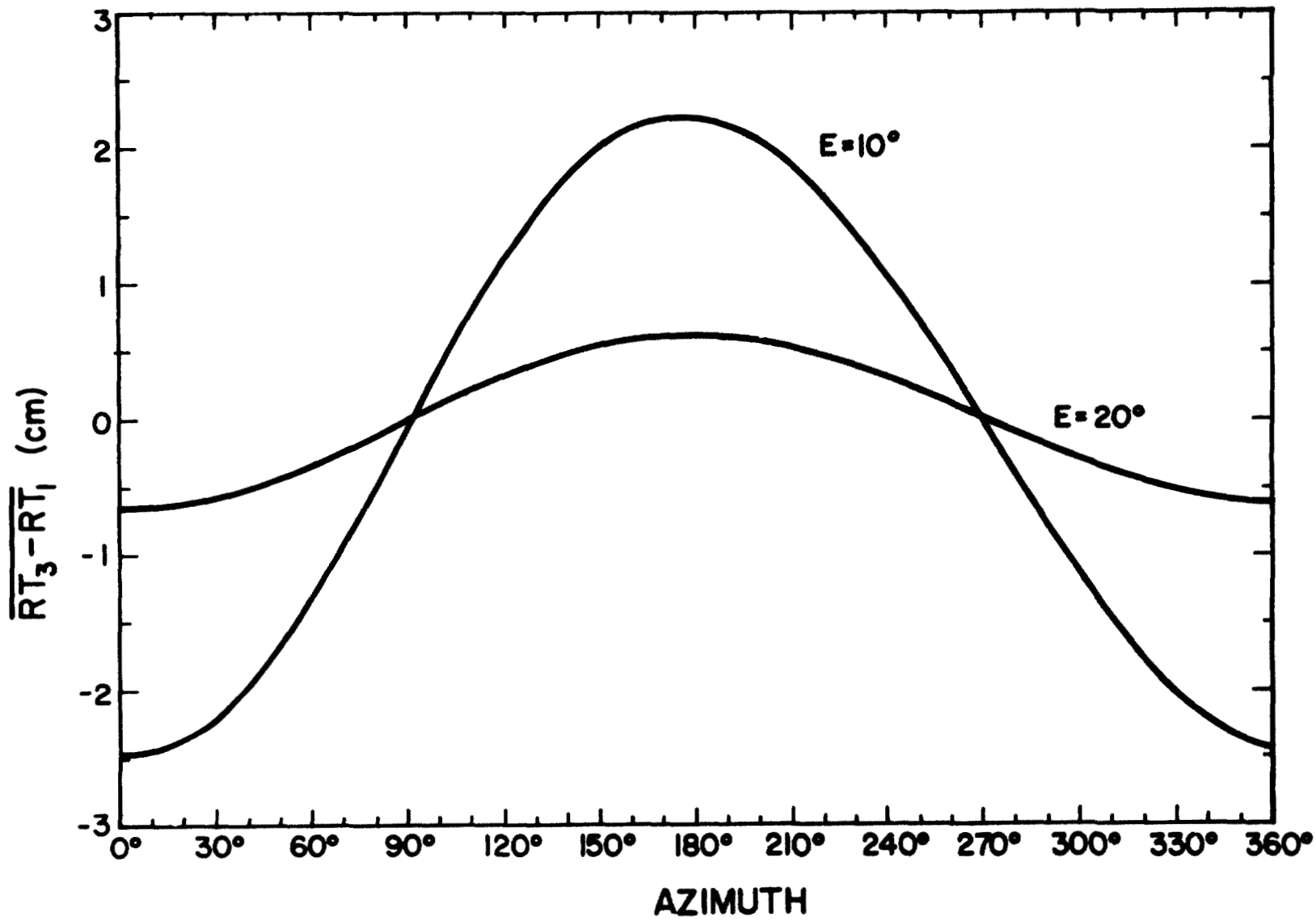


Figure 9. Mean of difference $RT_3 - RT_1$ versus azimuth at 10° and 20° elevation (31 sets of data).

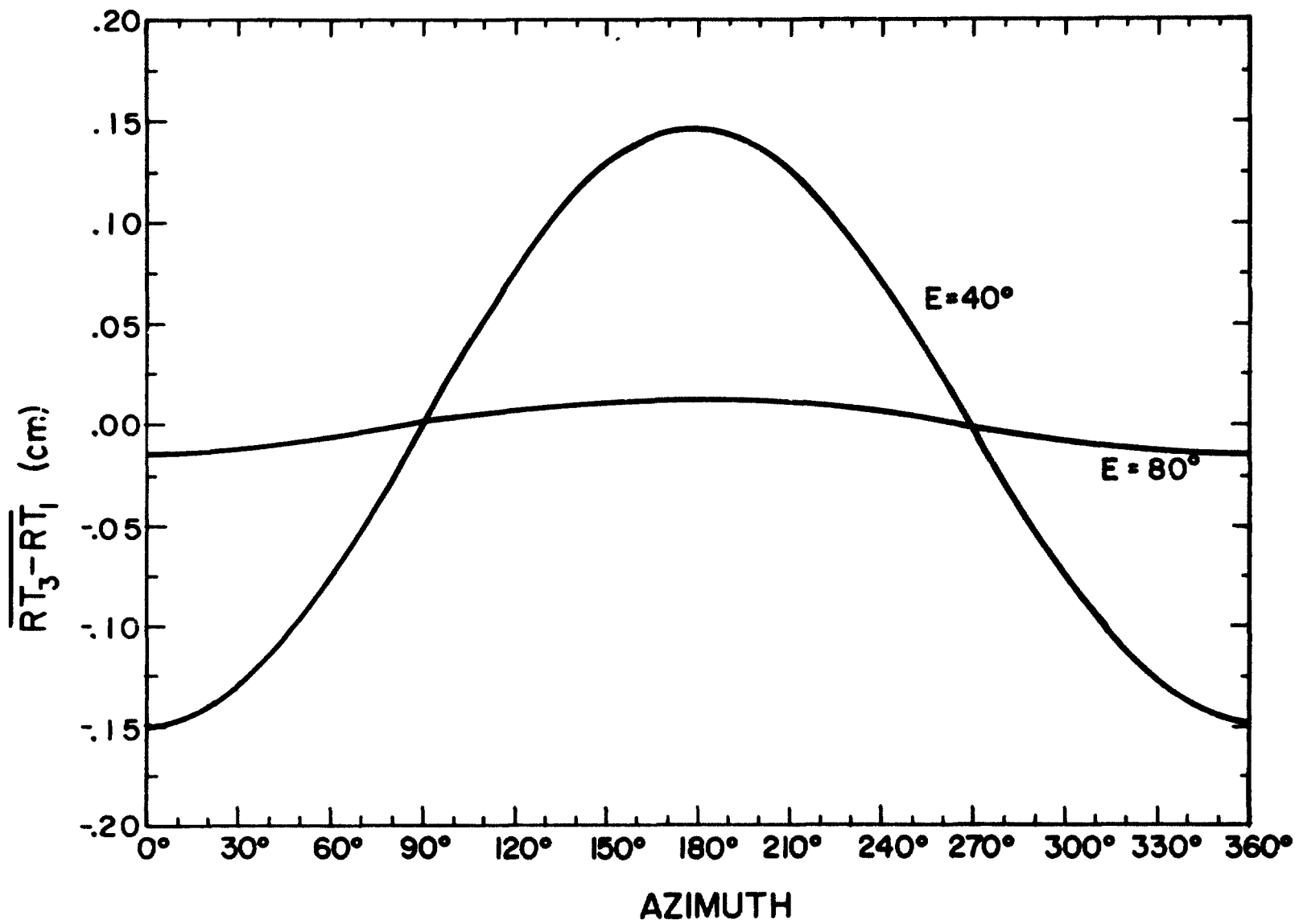


Figure 10. Mean of difference $RT_3 - RT_1$ versus azimuth at 40° and 80° elevation (31 sets of data).

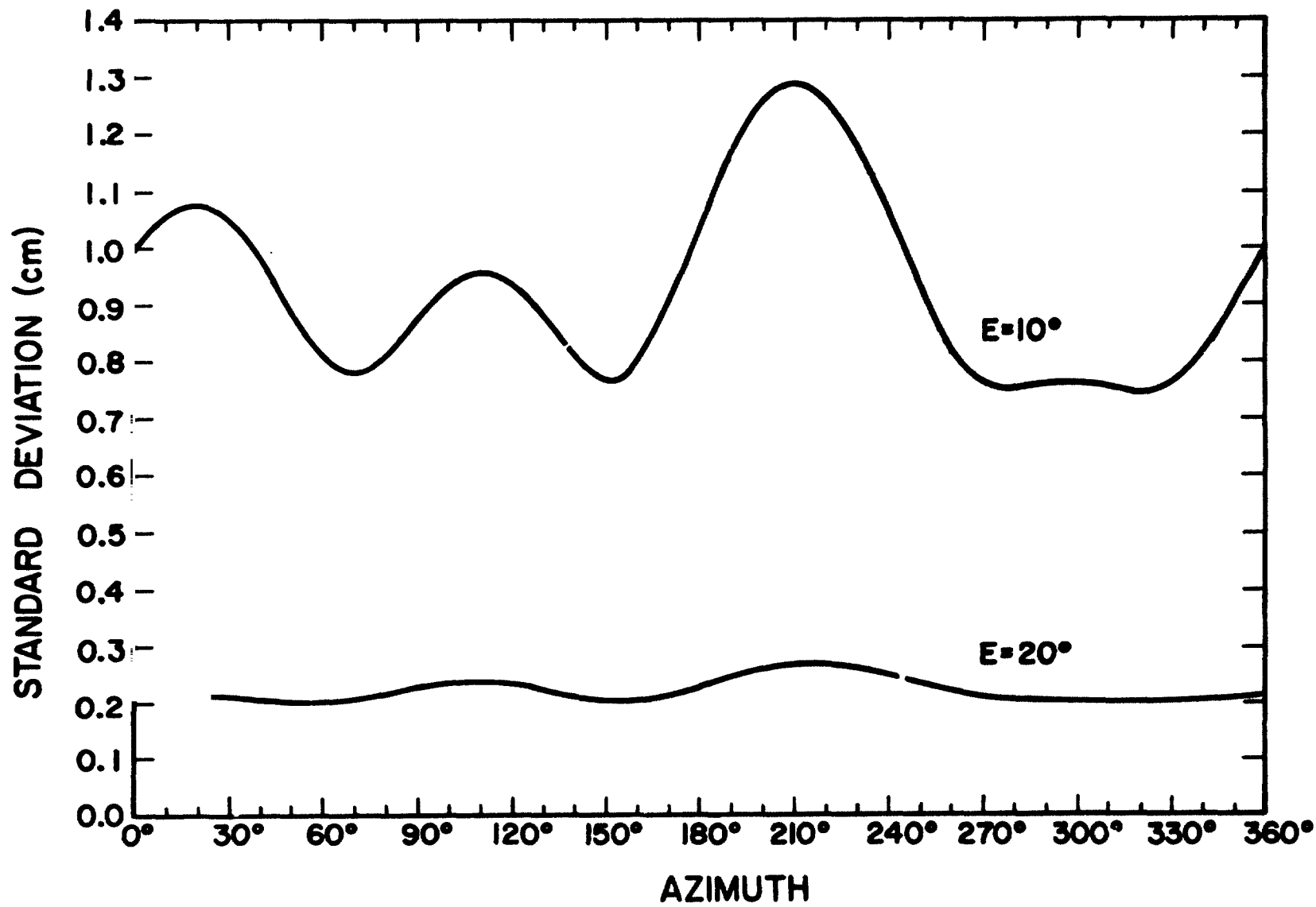


Figure 11. Standard deviation of difference $RT_3 - RT_1$ versus azimuth at 10° and 20° elevation (31 sets of data).

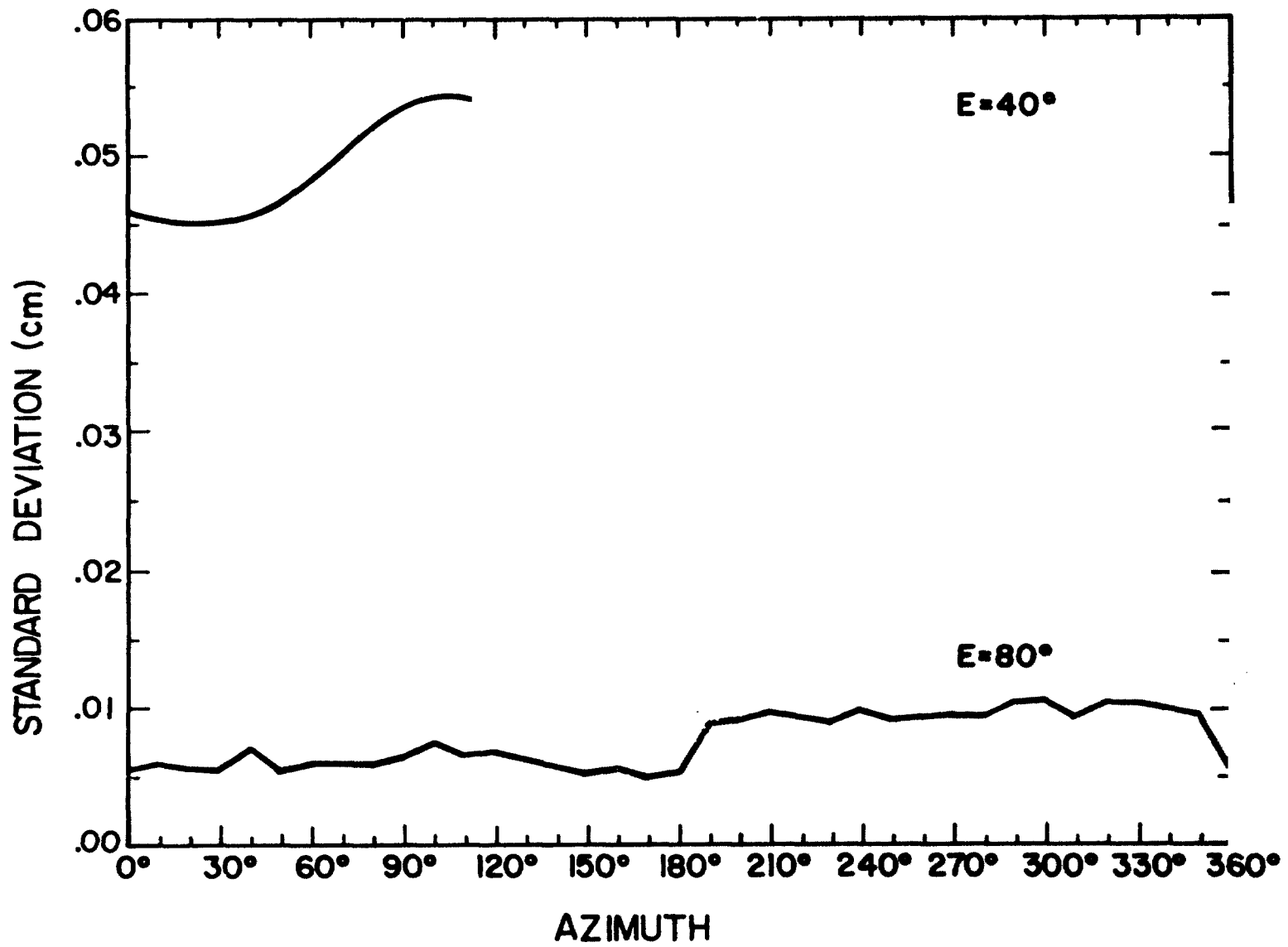


Figure 12. Standard deviation of difference $RT_3 - RT_1$ versus azimuth at 40° and 80° elevation (31 sets of data).

TABLE 4.

RESULTS OF THREE-DIMENSIONAL RAY TRACES
(31 sets, 1116 observations)

<u>Elev. Angle</u>	<u>RT₃ - RT₁</u>	
	<u>Mean</u>	<u>SD</u>
10°	-0.0666 cm	1.9009 cm
20°	-0.0079	0.4968
40°	-0.0008	0.1160
80°	-0.0005	0.0127

Histograms of $RT_3 - RT_1$ for the four elevation angles are plotted in Figures 13-16. Since $RT_3 - RT_1$ is approximately sinusoidal, one would expect the histograms to resemble the density function for a sinusoid with random phase and amplitude. For a fixed amplitude A and random phase θ uniformly distributed between 0 and 2π , the probability density $Y = A \sin \theta$ is given by

$$f_Y(y) = \begin{cases} \frac{1}{\sqrt{A^2 - y^2}} & |y| < A \\ 0 & \text{otherwise} \end{cases}$$

f_Y has peaks at $\pm A$ and a minimum at $y = 0$. However, the random amplitude A tends to smear the peaks. The smearing nearly obscures the peaks in the $E = 10^\circ$ histogram, but they are apparent at $E = 20^\circ$ and $E = 40^\circ$, where the amplitude varies less. The $E = 80^\circ$ histogram contains computer round-off noise.

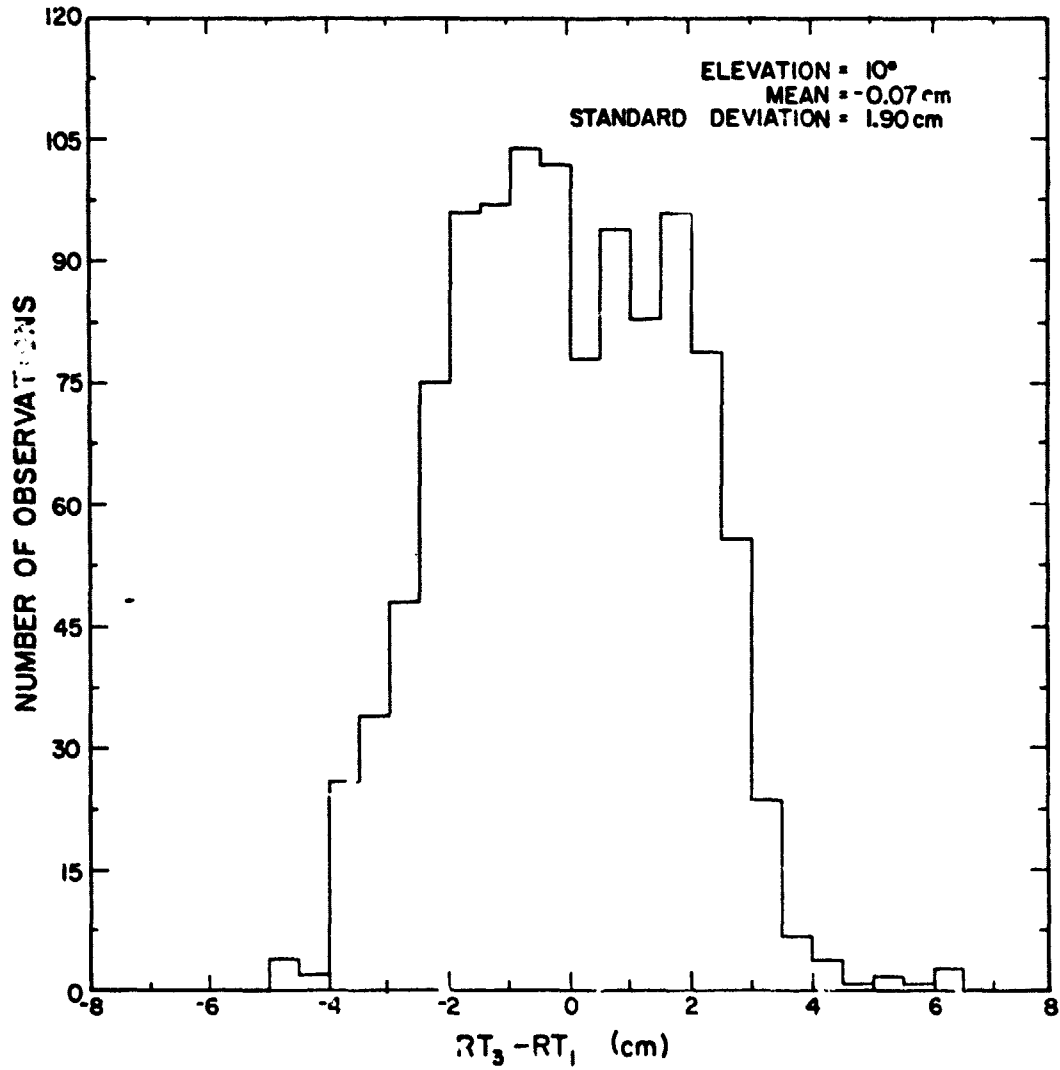


Figure 13. Histogram of difference $RT_3 - RT_1$ at 10° elevation (31 sets of data, 1116 observations).

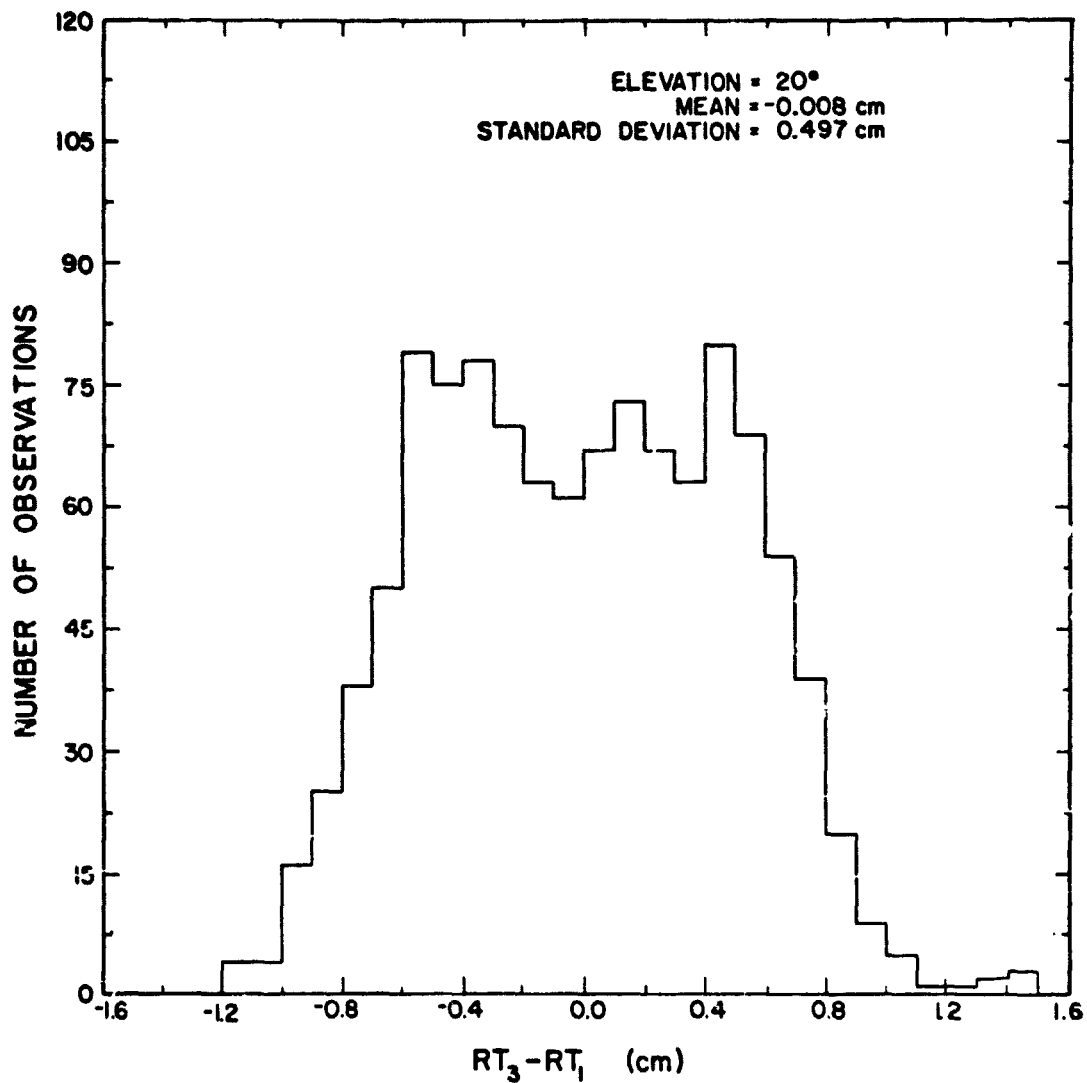


Figure 14. Histogram of difference $RT_3 - RT_1$ at 20° elevation (31 sets of data, 1116 observations).

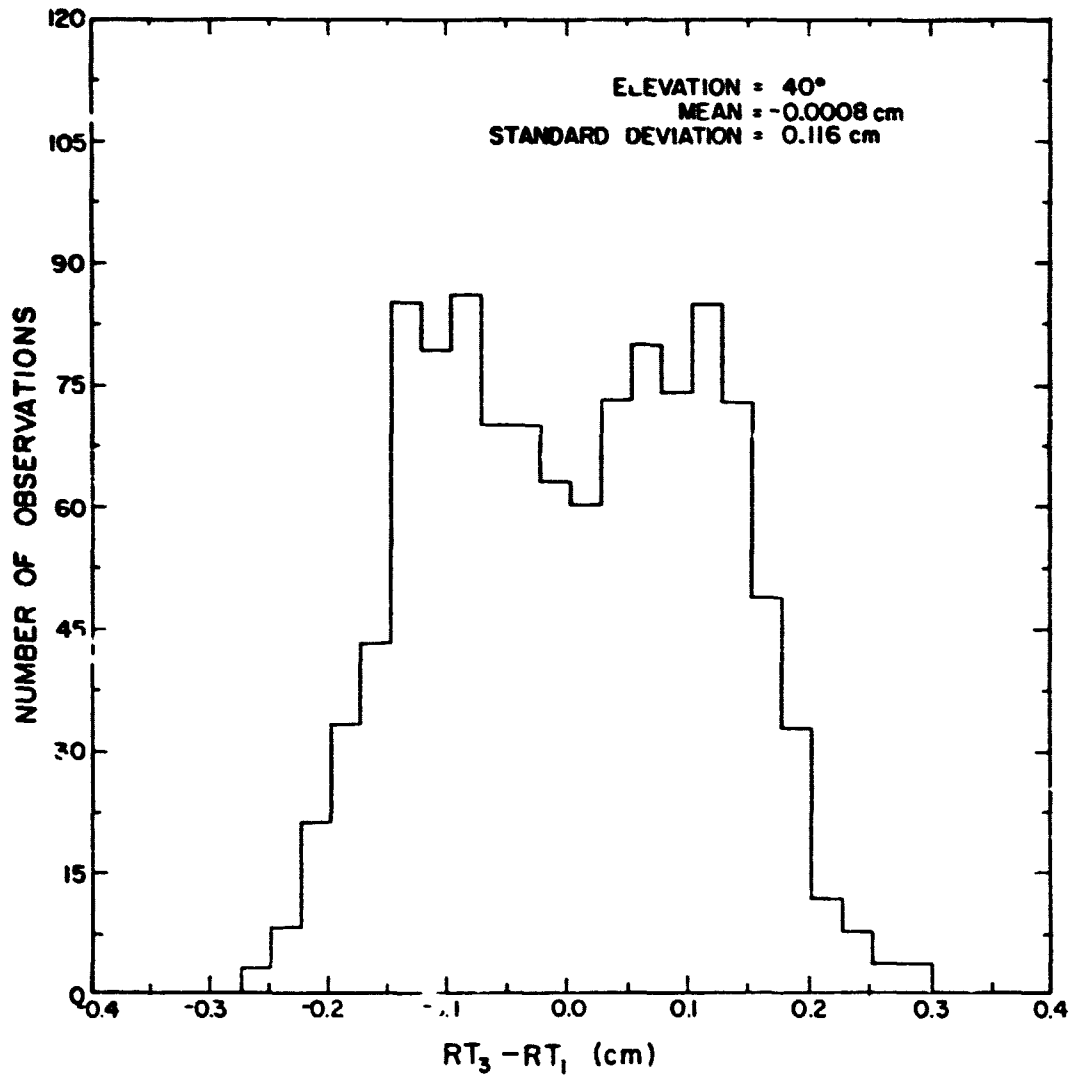


Figure 15. Histogram of difference $RT_3 - RT_1$ at 40° elevation (31 sets of data, 1116 observations).

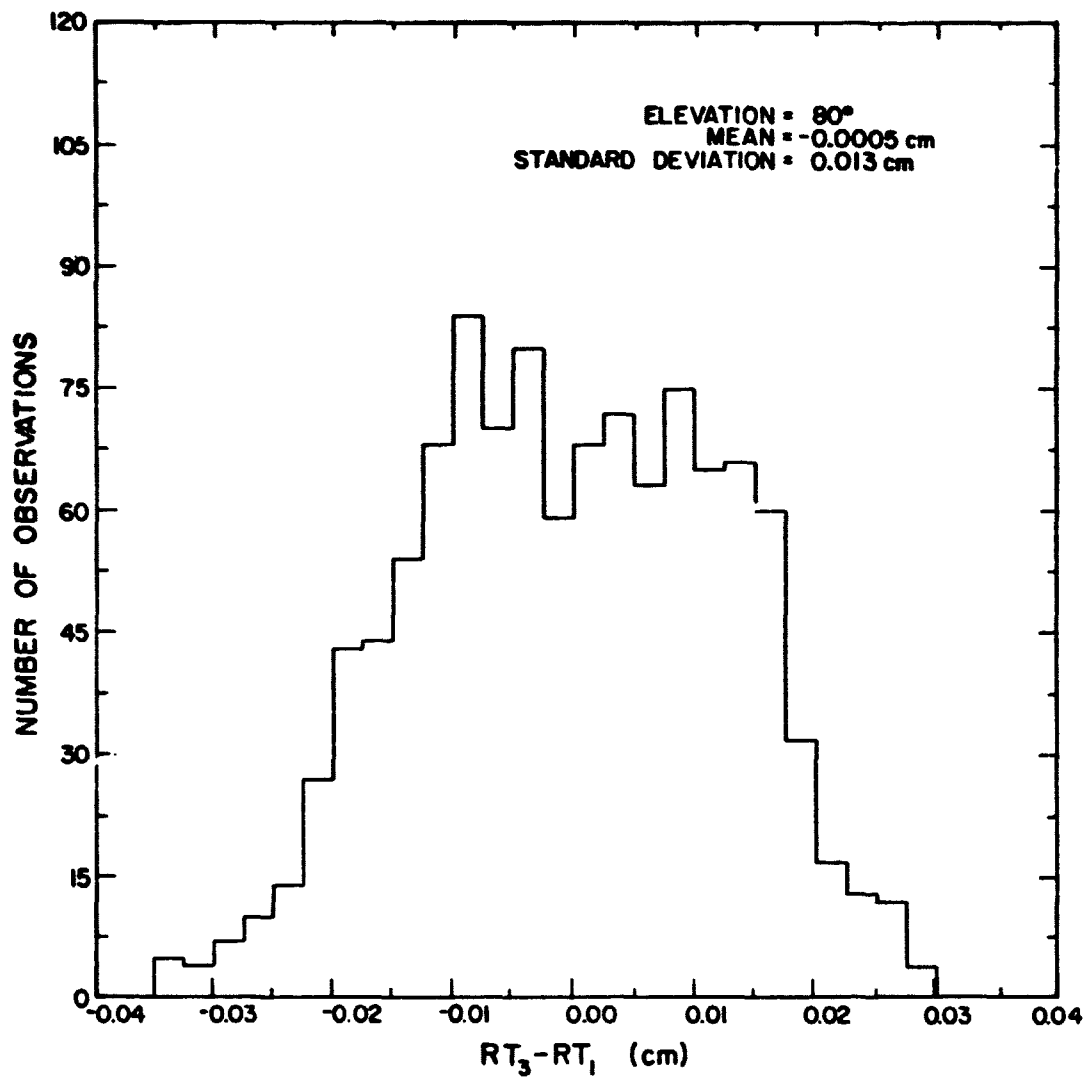


Figure 16. Histogram of difference $RT_3 - RT_1$ at 80° elevation (31 sets of data, 1116 observations).

6. CONCLUSION

The effects of horizontal refractivity gradients on the accuracy of laser ranging systems was investigated by ray tracing through three-dimensional refractivity profiles. The profiles were generated by performing a multiple regression on measurements from seven or eight radiosondes. The refractivity models provided for both linear and quadratic variations in the horizontal direction. To isolate the gradient effects the range calculated from a spherically symmetric ray trace (RT_1) was subtracted from the range calculated from the three-dimensional ray traces (RT_3). The mean of the difference $RT_3 - RT_1$ was a sinusoidal function of azimuth having a minimum near 0° azimuth (due north) and a maximum near 180° azimuth (due south). The peak-to-peak variation was approximately 5 centimeters at 10° elevation and decreased to about 3 millimeters at 40° elevation. The standard deviation of $RT_3 - RT_1$ was approximately 1 centimeter at 10° elevation and decreased to 0.5 millimeters at 40° elevation. The ray trace results also indicated that the linear variation of the refractivity in the horizontal direction is the primary error source in the range correction formulas. The effects of quadratic and higher-order variations appear to be negligible.

APPENDIX A.

APPROXIMATION OF $\frac{1}{\sin(\theta)}$

$$\frac{1}{\sin(\theta)} = \frac{1}{\sin(\theta_0)} \frac{1}{\left[\frac{1 - \left(\frac{n_0 r_0}{nr}\right)^2}{1 + \frac{1}{\tan^2(\theta_0)}} \right]^{1/2}} \quad (\text{A-1})$$

Consider $1 - \left(\frac{n_0 r_0}{nr}\right)^2$

$$\begin{aligned} 1 - \left(\frac{n_0 r_0}{nr}\right)^2 &= 1 - \left(1 + 10^{-6} N_0\right)^2 \left[\frac{r_0}{(1 + 10^{-6} N)(r_0 + h)} \right]^2 \\ &= 1 - \left(1 + 10^{-6} N_0\right)^2 \left[\frac{1}{1 + \left(10^{-6} N + \frac{h}{r_0} + 10^{-6} N \frac{h}{r_0}\right)} \right]^2 \\ &= 1 - \left(1 + 2 \times 10^{-6} N_0 + 10^{-12} N_0^2\right) \\ &\quad \cdot \sum_{i=0}^{\infty} (i+1) \left(-10^{-6} N - \frac{h}{r_0} - 10^{-6} N \frac{h}{r_0}\right)^i . \end{aligned}$$

Neglecting $10^{-12} N_0^2$ ($N_0 \approx 300$) and taking the first two terms of the series

$$1 - \left(\frac{n_0 r_0}{nr}\right)^2 \approx 1 - \left(1 + 2 \times 10^{-6} N_0\right) \left(1 - 2 \times 10^{-6} N - \frac{2h}{r_0} - 2 \times 10^{-6} N \frac{h}{r_0}\right) .$$

Taking only first-order terms,

$$1 - \left(\frac{n_0 r_0}{nr}\right)^2 \approx 2 \left[\frac{h}{r_0} - 10^{-6} (N_0 - N) \right] .$$

Now

$$\frac{1}{\sqrt{1+X}} \approx 1 - \frac{X}{2} + \frac{3X^2}{8} \text{ for } X \ll 1 .$$

Equation (A-1) can be written

$$\frac{1}{\sin(\theta)} \approx \frac{1}{\sin(\theta_0)} \left\{ 1 - \frac{\frac{h}{r_0} - 10^{-6}(N_0 - N)}{\tan^2(\theta_0)} + \frac{\frac{3}{2} \left[\frac{h}{r_0} - 10^{-6}(N_0 - N) \right]^2}{\tan^4(\theta_0)} \right\}.$$

APPENDIX B.

SIMPLIFICATION OF EQUATION (2-9)

Consider the $\frac{1}{\sin(E)}$ terms of Eq. (2-9)

$$\begin{aligned}
 & \frac{1}{\sin(E)} \left\{ 10^{-6} \int N_g dh + 10^{-6} \int \left[\frac{h}{r_0} - 10^{-6}(N_0 - N) \right] N_g dh \right. \\
 & \quad \left. + \frac{3}{2} \cdot 10^{-6} \int \left[\frac{h}{r_0} - 10^{-6}(N_0 - N) \right]^2 N_g dh \right\} \\
 &= \frac{10^{-6}}{\sin(E)} \left[1 - 10^{-6}N_0 + \frac{3}{2} \cdot 10^{-12}(N_0 - N)^2 \right] \int N_g dh \\
 & \quad + \frac{10^{-6}}{r_0 \sin(E)} \left[1 - 3 \times 10^{-6}(N_0 - N) \right] \int hN_g dh \\
 & \quad + \frac{10^{-12}}{\sin(E)} \int NN_g dh + \frac{\frac{3}{2} \cdot 10^{-6}}{r_0^2 \sin(E)} \int h^2 N_g dh \\
 &= \frac{10^{-6}}{\sin(E)} \left[1 - 10^{-6}N_0 \right] \int N_g dh + \frac{10^{-6}}{r_0 \sin(E)} \int hN_g dh + \frac{10^{-12}}{\sin(E)} \int NN_g dh \\
 & \quad + \frac{\frac{3}{2} \cdot 10^{-6}}{r_0^2 \sin(E)} \int h^2 N_g dh
 \end{aligned}$$

where $N_0 = 300 \geq N$, $E \geq 10^\circ$, and the evaluations [Eq. (2-11)] have been used to eliminate any terms contributing less than 1 mm. A similar analysis of the remaining terms gives

$$\begin{aligned}
 \Delta R &= \frac{1}{\sin(E)} \left\{ 10^{-6} \int N_g dh + 10^{-6} \int \left[\frac{h}{r_0} - 10^{-6}(N_0 - N) \right] N_g dh \right\} \\
 & \quad - \frac{1}{\sin^3(E)} \left\{ \frac{10^{-6}}{r_0} \int hN_g dh + 10^{-12} \int (NN_g - \frac{1}{2} N^2) dh + \frac{3 \times 10^{-6}}{r_0^2} \int h^2 N_g dh \right\} \\
 & \quad + \frac{1}{\sin^5(E)} \left\{ \frac{3}{2} \cdot \frac{10^{-6}}{r_0^2} \int h^2 N_g dh + \frac{3 \times 10^{-12}}{r_0} \int hNN_g dh \right\} \quad (B-1)
 \end{aligned}$$

Consider the following pair of terms of (B-1)

$$-\frac{3 \times 10^{-6}}{r_0^2 \sin^3(E)} \int h^2 N_g dh \approx \frac{-1.64 \times 10^{-5}}{\sin^3(E)}$$

$$\frac{3 \times 10^{-12}}{r_0 \sin^5(E)} \int h N N_g dh \approx \frac{6.92 \times 10^{-7}}{\sin^5(E)}$$

where the evaluations of (2-11) or Appendix C have been used, with

$N_0 \approx 300$, $P_s \approx 1000$ mb, $T_s \approx 273^\circ$ K, and $K \approx 0.9$.

At $E = 10^\circ$, the sum of these terms is about 1 mm, and they approximately cancel. At $E \geq 20^\circ$, each of the terms is individually less than 1 mm and they are thus insignificant. For $10^\circ < E < 20^\circ$ the sum of these terms is 1.00 mm or less. Leaving these terms out, (2-10) is obtained.

APPENDIX C.

INTEGRAL EVALUATIONS

$$1. \quad \int h^2 N_g \, dh$$

Approximating N_g by the dominant first term of (2-1),

$$\int h^2 N_g \, dh \approx \int h^2 (80.343) f(\lambda) \frac{P}{T} \, dh .$$

Marini and Murray use the hydrostatic equation to obtain [1, Appendix 2]

$$P = P_s \left(\frac{T}{T_s} \right)^{-\frac{Mg}{\beta R}}$$

$$\text{and } T = T_s + \beta h$$

where $M = 28.966 =$ molecular weight of dry air (kg)

$g = 9.8 =$ acceleration of gravity (m/s)

$R = 8314.36 =$ universal gas constant $\left(\frac{\text{joules}}{^\circ\text{K} - \text{kg-mole}} \right)$

$\beta =$ temperature lapse rate

$P_s, T_s =$ surface pressure and temperature.

$$\int h^2 N_g \, dh \approx 80.343 f(\lambda) \frac{P_s}{T_s} \int \left(\frac{T_s + \beta h}{T_s} \right)^{-\left(\frac{Mg}{\beta R} + 1 \right)} h^2 \, dh .$$

Integrating by parts twice, we obtain

$$\int h^2 N_g \, dh \approx 80.343 f(\lambda) \left(\frac{R}{Mg} \right)^3 P_s T_s^2 \frac{2K^2}{2 - K}$$

$$\text{where } K \equiv \frac{1}{1 - \frac{R\beta}{Mg}}$$

and so

$$\frac{3}{2} \cdot \frac{10^{-6}}{r_0^2} \int h^2 N_g \, dh \approx 1.4961 \cdot 10^{-13} f(\lambda) P_s T_s^2 \frac{K^2}{2 - K} .$$

$$2. \quad \int hNN_g dh$$

$$\text{Let } N = N_g = 80.343f(\lambda) \frac{P}{T},$$

$$\int hNN_g dh = \int (80.343)^2 f(\lambda) \frac{P^2}{T^2} h dh.$$

Integrating by parts,

$$\begin{aligned} \int hNN_g dh &\approx (80.343)^2 f(\lambda) \frac{P_s^2}{\beta T_s} \frac{1}{1 + \frac{2Mg}{RB}} \int \left(\frac{T_s + \beta h}{T_s} \right)^{-\left(\frac{2Mg}{RB} + 1\right)} dh \\ &\approx (80.343)^2 f(\lambda) P_s^2 \left(\frac{R}{2Mg} \right)^2 \frac{2}{3 - 1/K}. \end{aligned}$$

Thus we obtain

$$\frac{3 \times 10^{-12}}{r_0} \int hNN_g dh \approx 6.533 \times 10^{-13} P_s^2 \frac{2}{3 - 1/K}.$$

$$3. \quad 10^{-12} \int (N_0 - N)N_g dh$$

This integral divides into two terms which have been evaluated in [1]:

$$\begin{aligned} 10^{-12} \int (N_0 - N)N_g dh &= 10^{-6} N_0 \left(10^{-6} \int N_g dh \right) - 10^{-12} \int NN_g dh \\ &\approx 10^{-6} N_0 \left[.002357 P_s \frac{f(\lambda)}{f(\phi, H)} \right] \\ &\quad - 2 \times 4.7343 \times 10^{-8} f(\lambda) \frac{P_s^2}{T_s} \frac{2}{3 - 1/K} \end{aligned}$$

where the less significant terms have been ignored. Approximating N_0 :

$$N_0 \approx 80.343f(\lambda) \frac{P_s}{T_s}$$

we obtain

$$10^{-12} \int (N_0 - N) N_g dh = 9.4682 \times 10^{-8} \frac{P_s^2}{T_s} f(\lambda) .$$

APPENDIX D.

MARINI AND MURRAY'S SURFACE CORRECTION FORMULA

Marini and Murray [1] developed a surface correction formula using an analysis like that in Section 2. They considered only the three most significant terms of Equation 2-10 (the underlined terms), and obtained

$$MM = \frac{f(\lambda)}{F(\theta, H)} \cdot \frac{A + B^*}{\sin(E) + \frac{B/(A + B^*)}{\sin(E) + .01}}$$

where $A = 0.002357P_s + 0.000141e_s$

$$B = 1.0842 \times 10^{-8} P_s T_s K + 4.7343 \times 10^{-8} \frac{P_s^2}{T_s} \frac{2}{3 - 1/K}$$

and $f(\lambda)$, $F(\theta, H)$ and K are as defined in Section 2.

The starred B terms are an "optional adjustment" to reduce a bias at elevations near 90°. However, our investigation showed these terms to have a significant effect at all elevations. Including the starred B terms increases the value of MM by about 1.6 cm at 10° elevation, 0.8 cm at 20° elevation, 0.45 cm at 40° elevation, and 0.3 cm at 80° elevation. The starred B terms were neglected in our comparisons using Marini and Murray's formula.

REFERENCES

1. J. J. Marini and C. W. Murray, "Correction of laser range tracking data for atmospheric refraction at elevations above 10 degrees," NASA Tech. Rep. X-591-73-531, November 1973.
2. D. L. Zanter, C. S. Gardner and N. N. Rao, "The effects of atmospheric refraction on the accuracy of laser ranging systems," RRL Publication No. 471, University of Illinois, Urbana, Illinois, January 1976.
3. B. Carnahan, H. A. Luther and J. O. Wilkes, Applied Numerical Methods. New York: John Wiley & Sons, Inc., 1969.
4. S. Penn, G. J. Thompson (Capt., USAF) and P. A. Giorgio, "Meteorological conditions associated with CAT observations in Project Haven Hop," Air Force Surveys in Geophysics, No. 236, under contract AFCRL-72-0043, January 1972.
5. G. D. Thayer, "A rapid and accurate ray tracing algorithm for a horizontally stratified atmosphere," Radio Science, vol. 1, no. 2, pp. 249-252, February 1967.
6. J. Saastamoinen, "Contributions to the theory of atmospheric refraction," Bulletin Geodesique, vol. 105-107, pp. 279-298, 383-397, 13-34, 1972.
7. C. S. Gardner and B. E. Hendrickson, "Correction of laser ranging data for the effects of horizontal refractivity gradients," RRL Publication No. 478, University of Illinois, Urbana, Illinois, December 1976.